Available online at www.sciencedirect.com
ScienceDirect
Separation and Purification Technology 55 (2007) 246–255
Separation Purification Technology
www.elsevier.com/locate/seppur

# Screening of zeolite adsorbents for separation of hexane isomers: A molecular simulation study

R. Krishna*, J.M. van Baten

*Van't Hoff Institute for Molecular Sciences, University of Amsterdam, Nieuwe Achtergracht 166, 1018 WV Amsterdam, The Netherlands*

Received 3 November 2006; received in revised form 5 December 2006; accepted 6 December 2006

**Abstract**

Recent developments in Monte Carlo (MC) simulation techniques have enabled the accurate calculation of sorption isotherms of a variety of molecules in zeolites. Using the example of separation of isomers of hexane we demonstrate the power of MC simulations for screening of zeolite adsorbents for maximum separation selectivity. The simulations underline the exploitation of entropy effects during mixture sorption


*Keywords:* Zeolites; Monte Carlo simulations; Separation of hexane isomers; Configurational entropy; Separation selectivity; Entropy effects

## 1. Introduction

Zeolites are crystalline nanoporous materials that are widely used in the chemical industry as catalysts and adsorbents [1]. Zeolite crystals are incorporated into binders and used in the form of pellets in fixed or (simulated) moving bed reactors. Alternatively, zeolite crystals are coated on to a porous membrane support and used in (catalytic) membrane reactors and separation devices. More than 180 zeolite structures are known [2]; Fig. 1 shows some common topologies. AFI, MOR and LTL, consist essentially of uni-dimensional channels; MOR also has side pockets. MFI, ISV and BEA have intersecting channel structures. FAU, LTA, CHA and DDR consist of cages that connect to one another through windows; these windows may be large (FAU), or narrow (LTA, CHA, DDR). For any given separation or reaction duty, there is an optimum zeolite structure offering the maximum selectivity or reactivity; arriving at this optimum zeolite by experiments is often a demanding and time consuming exercise.

Recent development in Monte Carlo (MC) simulation techniques, coupled with the availability of high performance computing facilities, have enabled the determination of the adsorption characteristics of a variety of molecules in different zeolites with a reasonable degree of accuracy and reliability [3–7]. The major objective of this paper is to illustrate the potential of MC simulations in screening zeolites by considering an example of current interest, i.e. the separation of hexane isomers. We demonstrate that molecular simulations can provide insights into adsorption mechanisms, siting and orientation of molecules that are not available from experiments alone. Furthermore it is demonstrated how entropy effects during mixture sorption can be exploited to obtain maximum sorption selectivities. Such insights allow the development of more fundamental models for process design.

## 2. Separation of hexane isomers

Isomerization of alkanes, for the purposes of octane improvement, is a process of increasing importance in the petroleum industry [8–10]. Fig. 2a shows an example of a process for isomerization of *n*-hexane (nC6). The product from the isomerization reactor, that commonly uses MOR as catalyst, consists of an equilibrium distribution of unreacted nC6, along with its mono-branched isomers 2-methylpentane (2MP), 3-methylpentane (3MP) and di-branched isomers 2,2-dimethylbutane (22DMB) and 2,3-dimethylbutane (23DMB). In current practice the linear nC6 is separated from the branched isomers in an adsorption separation step that relies on molecular sieving. The adsorbent is LTA zeolite that consists of cages separated by narrow (5 Å size) windows. The windows only allow the diffusion, and adsorption of the linear isomer, and the branched isomers are rejected and removed as product. The unreacted nC6 is recycled back to the reactor.

* Corresponding author. Tel.: +31 205257007; fax: +31 20 5255604.
*E-mail address:* r.krishna@uva.nl (R. Krishna).

1383-5866/$ – see front matter © 2006 Elsevier B.V. All rights reserved.
doi:10.1016/j.seppur.2006.12.011

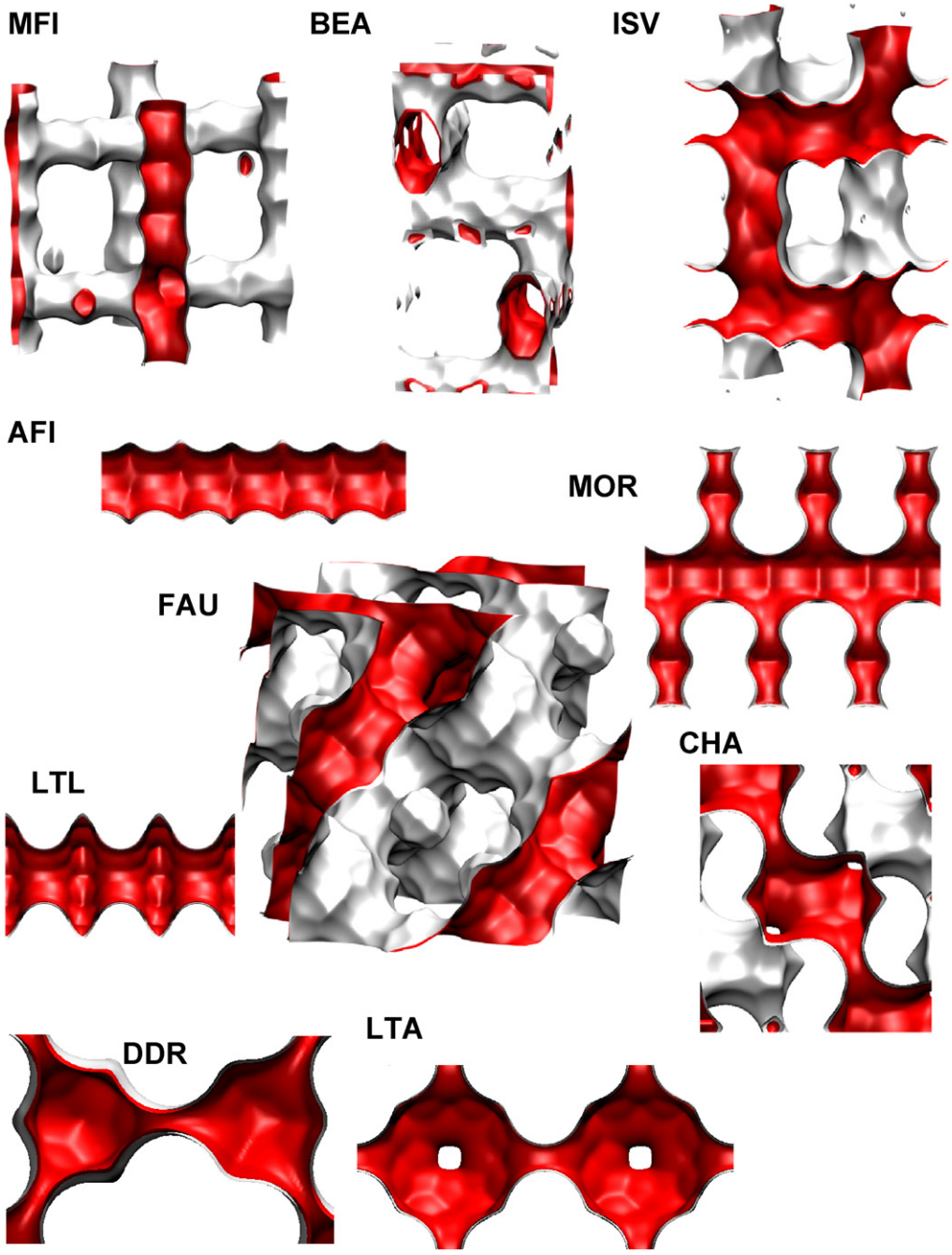


Fig. 1. A selection of zeolite structures.

The octane number increases with the degree of branching and so di-branched isomers are preferred products. An improved process (Fig. 2b) would require the recycle of both linear and mono-branched isomers to the reactor. The separation of 22DMB and 23DMB from the remaining isomers is a difficult task because it requires distinguishing molecules on the *degree* of branching. There are indications from the patent literature that this separation can be achieved using a zeolite adsorbent and a wide variety of zeolites are mentioned as candidate adsorbents [9,10]. We shall demonstrate how molecular simulations can provide clues to arriving at the choice of the optimum zeolite for this separation task. For illustration purposes and simplification of the discussions we consider the problem of separating a mixture consisting of nC6, 2MP and 22DMB.

The first task is to determine the pure component isotherms. Pure component adsorption isotherms can be measured experimentally; Fig. 3a show the measurements of Song and Rees [11] for *n*-hexane (nC6) in MFI (silicalite-1) at various temperatures; the data is plotted using linear scales on both axes, as is commonly done in practice. The experimental data at 336 K indicate a saturation capacity $q_{i,sat} \approx 1.4$ mol/kg. The volume of one unit cell of MFI is 5332 Å$^3$ and the framework density if 1796 kg m$^{-3}$. The saturation capacity of 1.4 mol/kg converts to a value of 8 molecules per unit cell. The data at

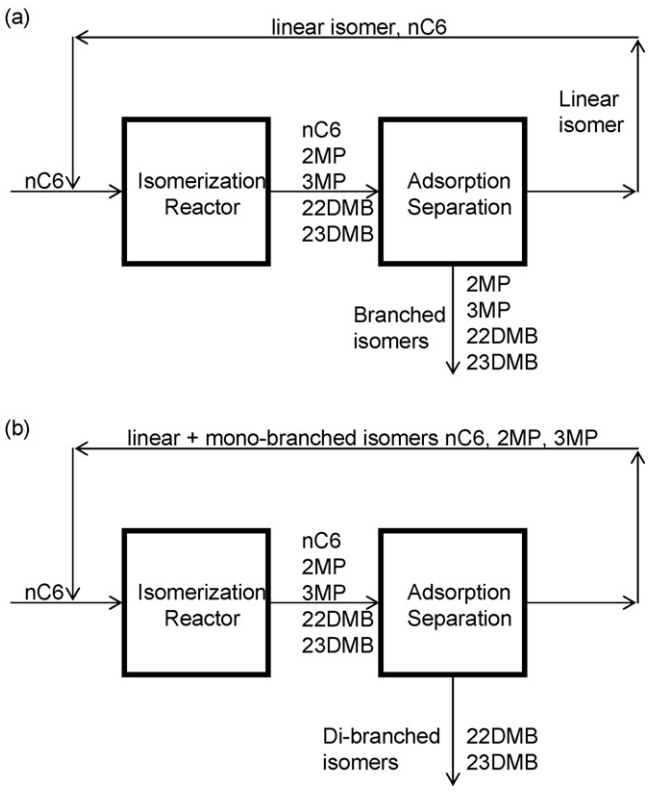


Fig. 2. (a) Conventional process flowsheet for alkane isomerization. (b) Improved process for alkane isomerization.

higher temperatures have not reached saturation limits, as is evident when the data is re-plotted using logarithmic scale for the pressure axis (see Fig. 3b). Also plotted in Fig. 3b are the configurational-bias Monte Carlo (CBMC) simulations results at 373 and 398 K; there is good agreement with the corresponding experimental data. The details of the CBMC simulation methodology are available in earlier publications [12–18]. In these simulations the zeolite framework is assumed to be rigid. The length of the nC6 molecule is commensurate with the distance between intersections along the zig-zag channels and a maximum of 8 molecules in a unit cell can be accommodated in the straight and zig-zag channels; Fig. 3c shows a snapshot of the location of molecules. Two points emerge from the results presented in Fig. 3. Firstly, the isotherm data should be plotted with logarithmic pressure scale in order to check whether the experiments have reached the saturation limits. Secondly, CBMC simulations allow accurate estimation of adsorption isotherms *up to saturation limits* for any temperature; this has been verified by extensive comparison of experimental data for a variety of alkanes, both linear and branched, in several zeolites [13,19].

CBMC simulations of the isotherms for nC6 are compared with that of its mono-branched isomer 2-methylpentane (2MP), and di-branched isomer (22DMB) in MFI at 433 K in Fig. 4a. The simulations need to be carried out to pressures of the order of $10^{10}$ Pa in order to reach saturation limits for 2MP. Since the simulations are performed in the grand canonical (GC) ensemble, the chemical potentials are fixed and the values on the $x$-axis

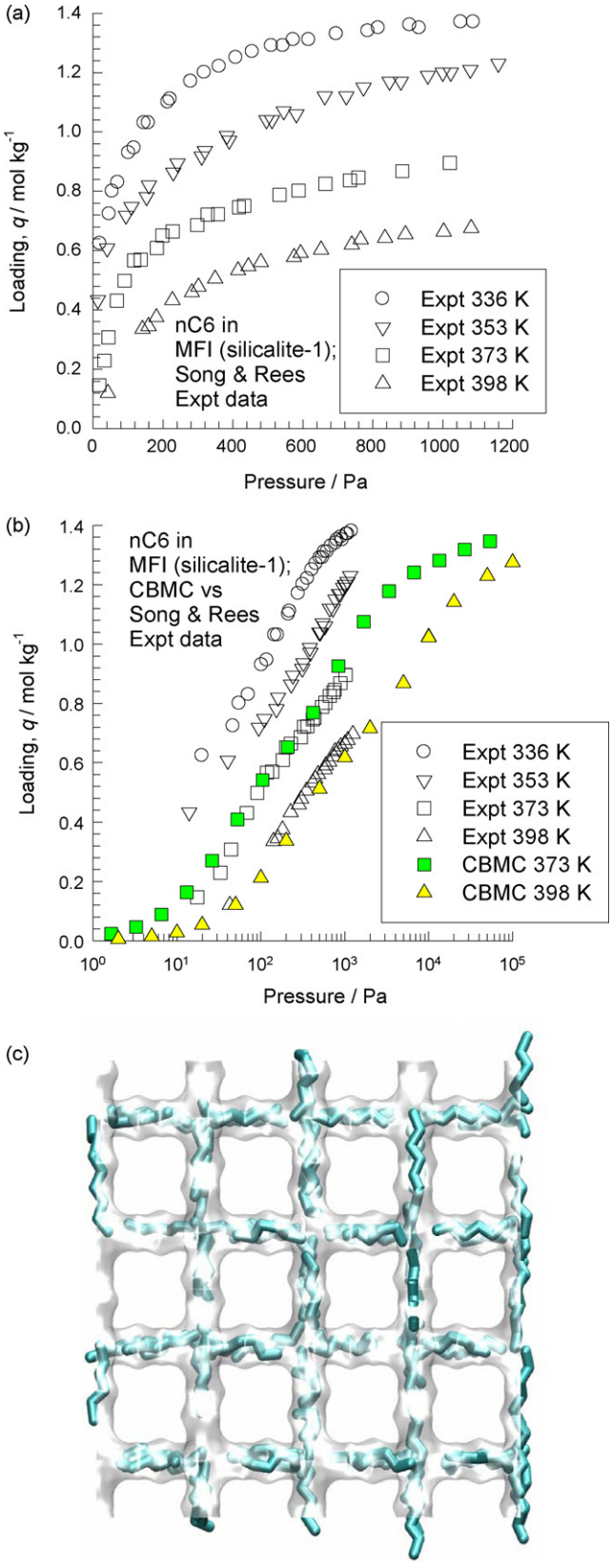


Fig. 3. (a) Experimental data of Song and Rees [11] for nC6 isotherms in MFI at various temperatures. (b) Comparison of experimental data with CBMC simulations at 373 and 398 K. (c) Snapshots showing the location of nC6 molecules within the straight and zig-zag channels of MFI at $T = 433$ K, $f = 100$ kPa.

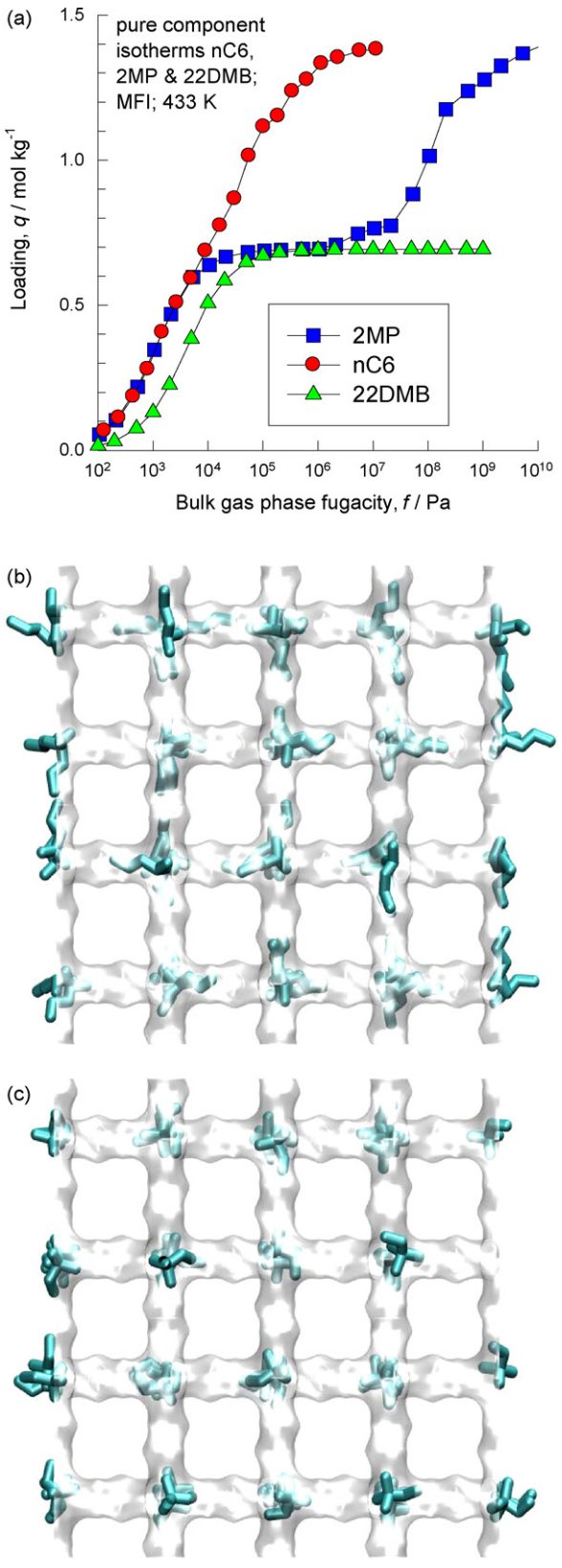


Fig. 4. (a) CBMC simulations of the pure component isotherms for nC6, 2MP and 22DMB in MFI at 433 K. (b) Snapshots showing the location of 2MP molecules within the straight and zig-zag channels of MFI at $T = 433$ K, $f = 100$ kPa; (c) Snapshots showing the location of 22DMB molecules within the straight and zig-zag channels of MFI at $T = 433$ K, $f = 100$ kPa.

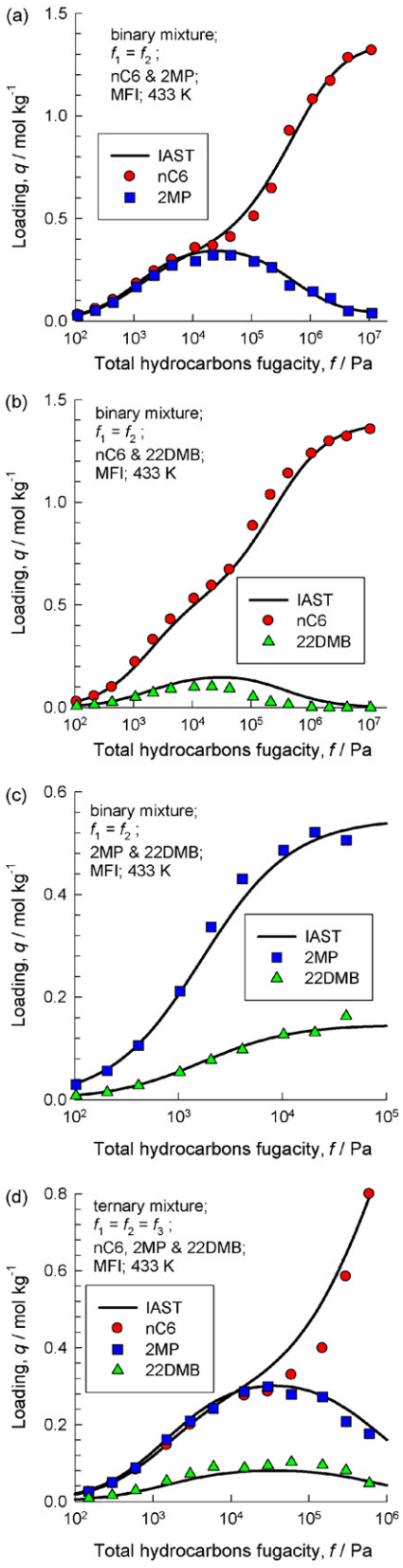


Fig. 5. CBMC simulations of loadings in the adsorbed phase in equilibrium with equimolar binary and ternary gas phase containing (a) nC6–2MP, (b) nC6–22DMB, (c) 2MP–22DMB and (d) nC6–2MP–22DMB mixtures in MFI at 433 K. The continuous solid lines represent calculations of the IAST [20] using dual-site Langmuir fits of pure component isotherms in Fig. 4.

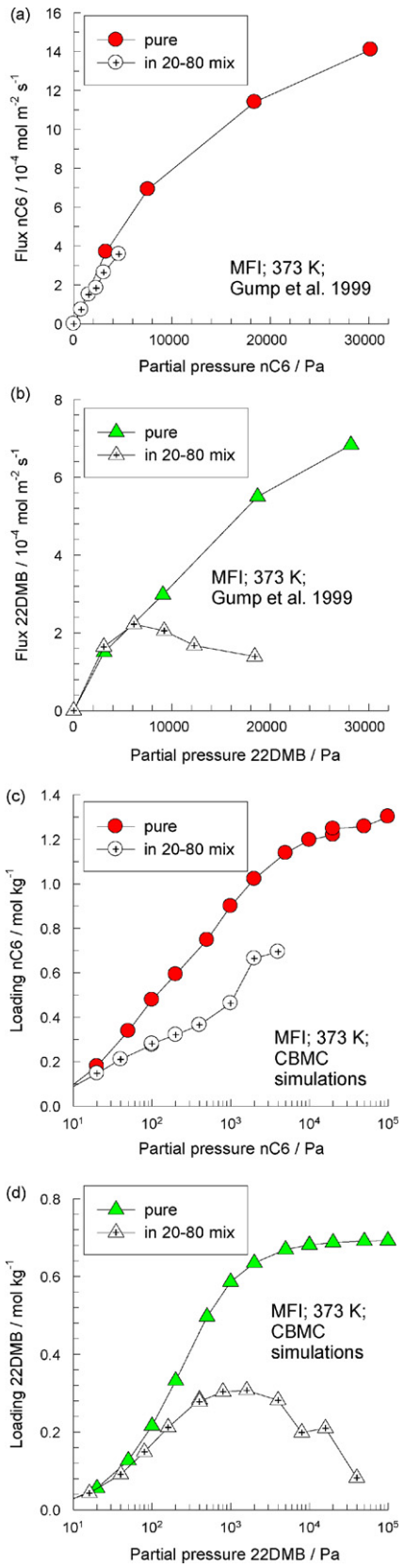


Fig. 6. Fluxes of (a) nC6 and (b) 22DMB for pure component and binary 20–80 mixture permeation across MFI membrane at 373 K. The experimental data are from Gump et al. [21]. CBMC simulations of (c) nC6 and (d) 22DMB loadings in the adsorbed phase in equilibrium with pure and binary 20–80 gas mixture at 373 K.

are properly the fugacities, $f$. There is a sharp inflection in the 2MP isotherm at $q = 0.7$ mol/kg, corresponding to 4 molecules per unit cell. The reason for this is that 2MP prefers to locate at the intersections due to the availability of extra "leg room"; see the snapshot in Fig. 4b. There are four intersections per unit cell of MFI. To obtain loading higher $q = 0.7$ mol/kg an extra push is required to make the mono-branched locate within the channel interiors; this extra push is the cause of the inflection in the isotherm. 22DMB also prefers to locate at the intersections of MFI because of leg room considerations; see Fig. 4c. However, 22DMB is more compact and cannot be pushed into the channel interiors; the saturation capacity is therefore limited to 4 molecules per unit cell.

The stark differences in the pure component adsorption behaviors of nC6, 2MP and 22DMB can be exploited to separate mixtures containing these species. CBMC simulations

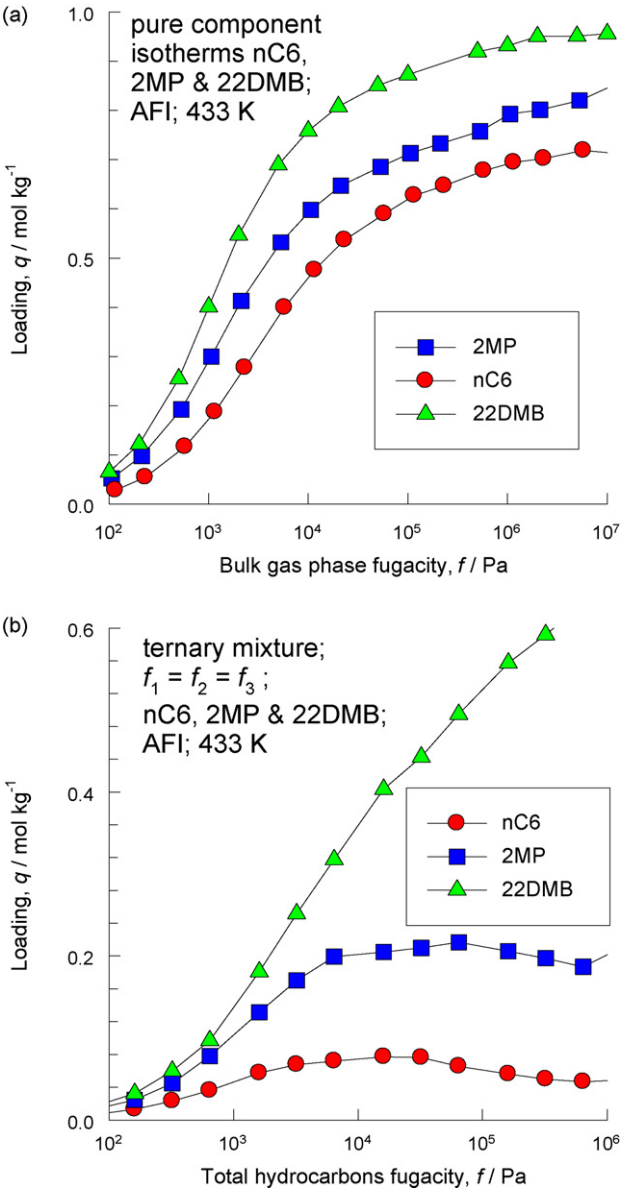


Fig. 7. (a) Pure component isotherms of nC6, 2MP and 22DMB in AFI at 433 K. (b) Component loadings in equilibrium with an equimolar ternary gas mixture.

of loadings in the adsorbed phase in equilibrium with equimolar binary and ternary gas phase containing (a) nC6–2MP, (b) nC6–22DMB, (c) 2MP–22DMB and (d) nC6–2MP–22DMB mixtures are shown in Fig. 5. Consider the nC6–2MP mixture. Up to a total hydrocarbons pressure of 50 kPa, the component loadings of both components increase in an expected manner. At 50 kPa pressure the total loading in the zeolite ≈ 0.7 mol/kg corresponding to 4 molecules per unit cell. All the intersection sites are fully occupied. To further adsorb 2MP we need to provide an extra "push". Energetically, it is more efficient to obtain higher mixture loadings by "replacing" the 2MP with nC6; this *configurational entropy* effect is the reason behind the curious maxima in the 2MP loading in the mixture. A similar behavior is observed for the nC6–22DMB mixture; see Fig. 5b. Since 2MP and 22DMB both compete for intersection sites, there is no corresponding maximum to be detected in the component loadings for the 2MP–22DMB mixture; see Fig. 5c. For adsorption of an equimolar ternary nC6–2MP–22DMB mixture, maxima in the component loadings of both 2MP and 22DMB are observed; see Fig. 5d.

From the point of view of separating hexane isomers we note that the highest separation selectivities are obtained at mixture loadings in excess of 0.7 mol/kg beyond which configurational entropy effects dominate mixture sorption and mandate the hierarchy nC6 ≫ 2MP ≫ 22DMB.

The continuous solid lines in Fig. 5 are the calculations following the ideal adsorbed solution theory (IAST) of Myers and Prausnitz [20] using dual-Langmuir fits of the pure component isotherms; this theory is able to capture the entropy effects quantitatively and can be used in process design calculations. It must be noted here that the commonly used multicomponent Langmuir isotherm will be unable to predict maxima in the loadings of the branched isomers as observed in Fig. 5a, b and d. This is because the sorption selectivity for the multicomponent Langmuir model is simply the ratio of the Langmuir constants, $b_i/b_j$, and is therefore independent of pressure; no maximum in component loading is anticipated.

Experimental confirmation of the maximum observed in the loading of the branched isomer in a binary mixture with nC6 is to be found in the MFI permeation experiments at 373 K reported by Gump et al. [21]. The fluxes of nC6 and 22DMB for pure component and binary 20–80 mixture permeation across MFI membrane at 373 K are shown in Fig. 6a and b as a function of the upstream hydrocarbons partial pressure. The pure component permeation fluxes behave as expected; increase in the upstream hydrocarbons pressure leads to an increasing flux. For the 20–80 mixture, the 22DMB permeation exhibits a maximum at upstream $p_{22DMB} \approx 5$ kPa. This curious maximum in 22DMB permeation flux is to be attributed to configurational entropy effects. For a 20–80 nC6–22DMB mixture, at $p_{22DMB} = 5$ kPa the total loading ≈0.7 mol/kg (see CBMC simulation data in Fig. 6c and d), and all the intersection sites are occupied. Further *increase* in the upstream pressure of the membrane leads to a *decrease* in the 22DMB loading, and consequently its flux. The separation selectivity increases sharply in favor of the linear isomer nC6 for loadings >0.7 mol/kg. The CBMC simulations provide a qualitative explanation of the observed maximum in the 22DMB flux. For proper modeling of the permeation fluxes, we also need to account for diffusion of the individual complexes, as has been shown in earlier work [22,23]. There is also experimental evidence of the validity of the ternary mixture predictions shown in Fig. 5d; see Santilli [24] and Calero et al. [25].

The pure component isotherms for AFI, that consists of unidimensional 12-ring channels of 7.3 Å size, shows a completely different sorption hierarchy than in MFI; see Fig. 7a. The dibranched isomer has the highest adsorption strength and the linear nC6 the lowest. As seen in Fig. 7b the component loadings for an equimolar ternary gas mixture show higher separation selectivities in favor of the component with the largest degree of branching, exactly opposite to that observed for MFI. The explanation can be found in the snapshots in Fig. 8. The linear nC6 has a longer "footprint" and occupies a longer segment of the channel; the 22DMB is the most compact molecule and has the smallest footprint. Consequently, more molecules of 22DMB can be located within a given length of AFI channel; this *molecular length entropy* effect dictates the sorption hierarchy. Analogous length entropy effects dictate the sorption hierarchy within MOR zeolite as can be witnessed from the pure component isotherms, and the corresponding snapshots, in Fig. 9. The equilibrium data for an equimolar ternary mixture in MOR is shown in Fig. 10. As in the case of AFI, both nC6 and 2MP exhibit a maximum

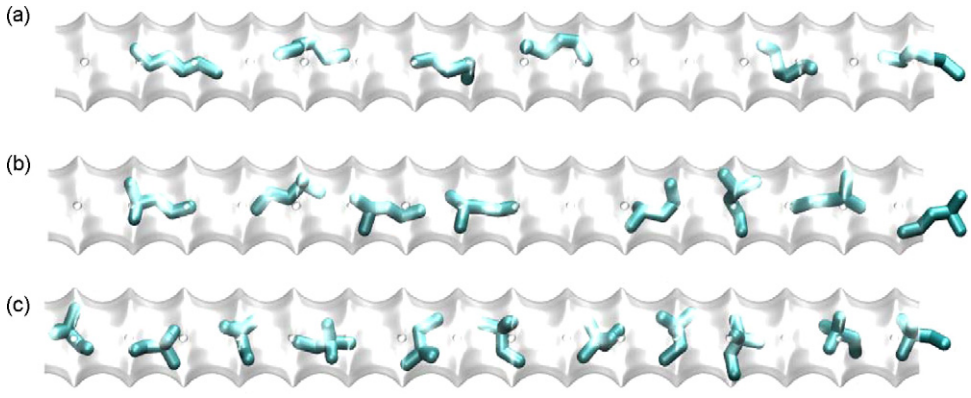


Fig. 8. Snapshots at 100 kPa and 433 K showing the location of (a) nC6, (b) 2MP and (c) 22DMB molecules in the 12-ring channels of AFI.

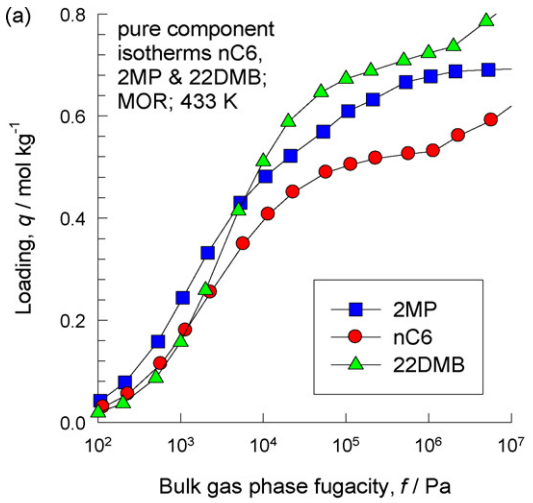


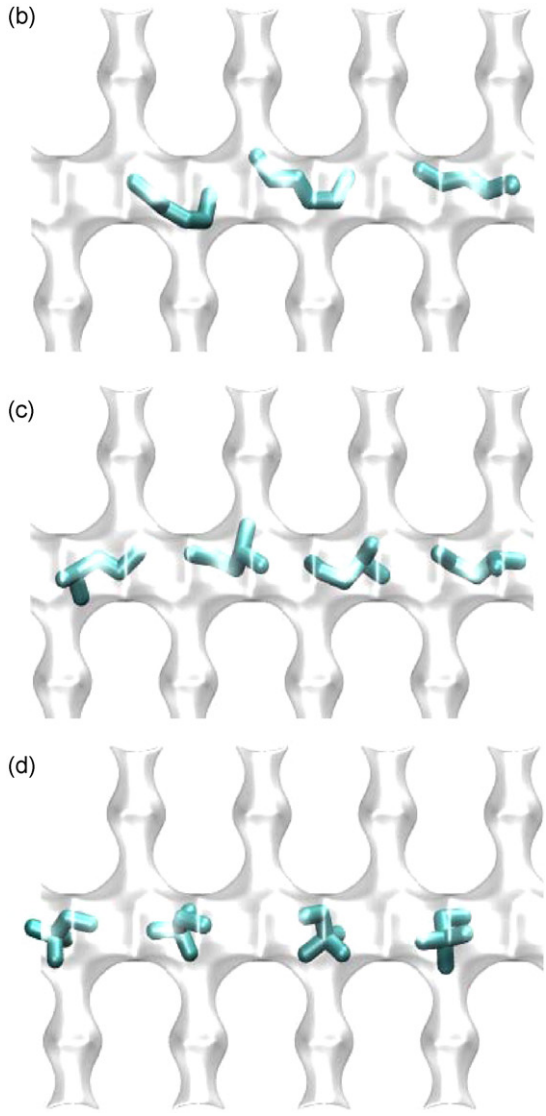


Fig. 9. (a) Pure component isotherms of nC6, 2MP and 22DMB in MOR at 433 K. Snapshots at 100 kPa and 433 K showing the location of (b) nC6, (c) 2MP and (d) 22DMB molecules in 12-ring channels of MOR.

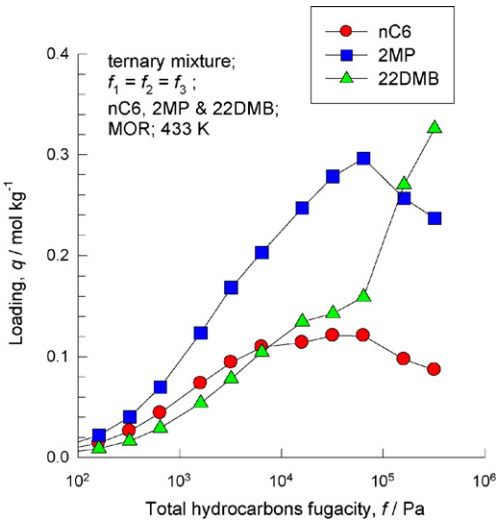


Fig. 10. Component loadings in equilibrium with an equimolar ternary gas mixture containing nC6, 2MP and 22DMB in MOR at 433 K.

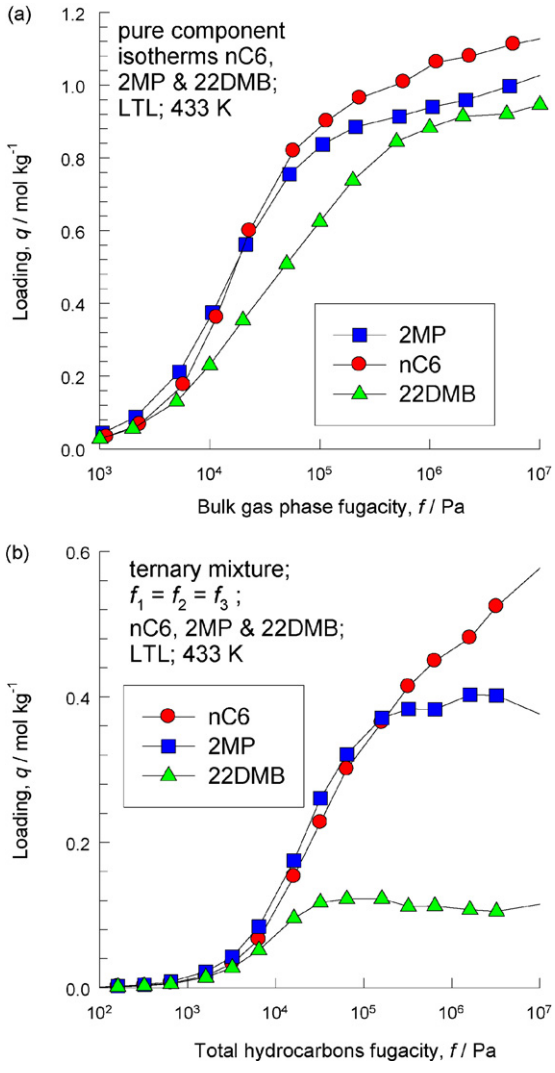


Fig. 11. (a) Pure component isotherms of nC6, 2MP and 22DMB in LTL at 433 K. (b) Component loadings in equilibrium with an equimolar ternary gas mixture.

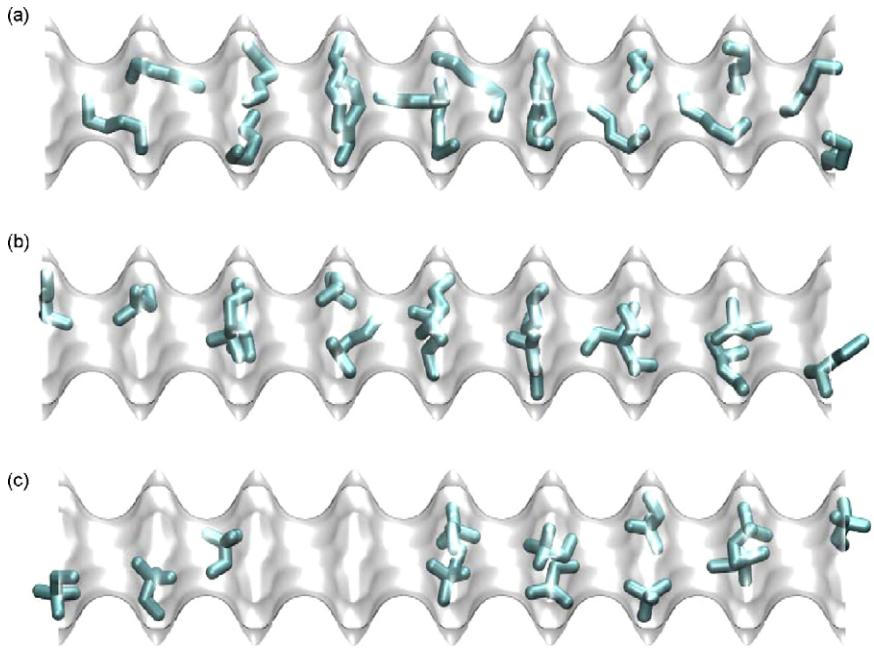


Fig. 12. Snapshots at 100 kPa and 433 K showing the location of (a) nC6, (b) 2MP and (c) 22DMB molecules in LTL.

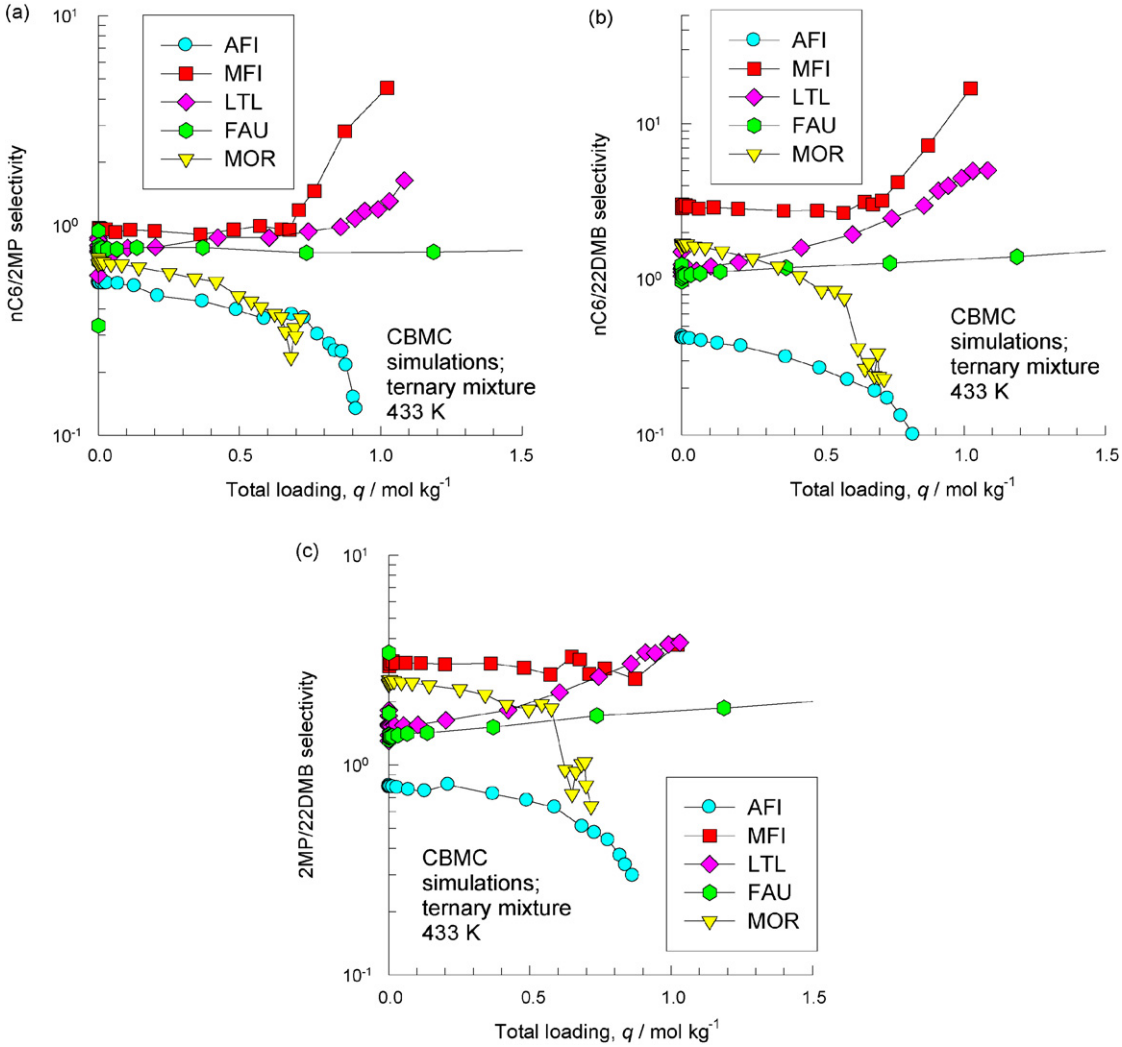


Fig. 13. (a) nC6/2MP, (b) nC6/22DMB and (c) 2MP/22DMB selectivities in MFI, MOR, FAU, AFI and LTL. The values are based on equimolar ternary mixture simulations at 433 K.

in the component loading and the component loading of 22DMB increases monotonically with increased pressure. The reason behind these maxima is that the "entropy battle" is lost successively by nC6 and 2MP to 22DMB that has the smallest footprint.

Adsorption of hexane isomers within the uni-dimensional channels of LTL produces a hierarchy that is different from that in AFI and MOR; see the pure component isotherms and the ternary equilibrium data in Fig. 11a and b. The explanation can be found in the snapshots in Fig. 12. The linear nC6 molecule can align across the channel and therefore has no "footprint disadvantage" with respect to the branched isomers.

The complete set of CBMC simulation results, in graphical form, for pure component, binary mixture and ternary mixtures of hexane isomers in MFI, AFI, MOR, LTL and FAU, along with snapshots, are available in Supplementary Data accompanying this publication. The nC6/2MP, nC6/22DMB and 2MP/22DMB selectivities in the ternary mixture are compared in Fig. 13a–c. The large pore FAU does not distinguish between the hexane isomers and all three selectivities are about unity. AFI and MOR zeolite both show selectivities in favor of the branched molecule that has a smaller footprint. Based on molecular simulation results we conclude that highest selectivities in favor of the linear nC6 and decreasing with the degree of branching is obtained in MFI; these high selectivities can be exploited to obtain sharp separations in chromatographic and moving bed adsorber configurations [23,26,27].

## 3. Conclusions

In this paper we have attempted to demonstrate the potential uses of MC simulations in the screening of zeolite adsorbents for separation of hexane isomers. MC simulations can be invaluable adjuncts to experiments, and allow isotherm data to be produced up to saturation conditions often difficult to achieve in experiments, especially for small molecules. In the case of mixtures, experimental data are very scarce [28] and MC simulations are invaluable in unraveling entropy effects arising out of differences in packing efficiencies of molecules, caused by subtle differences in configuration or size of their footprints.

## Acknowledgements

R.K. and J.M.vB. acknowledge the grant of a TOP subsidy from the Netherlands Foundation for Fundamental Research (NWO-CW) for intensification of reactors and NWO/NCF for provision of high performance computing resources. The CBMC simulations were carried out with the BIGMAC program developed by Dr. T.J.H. Vlugt.

## Appendix A. Supplementary data

Supplementary data associated with this article can be found, in the online version, at doi:10.1016/j.seppur.2006.12.011.

## References

[1] J. Kärger, D.M. Ruthven, Diffusion in Zeolites and Other Microporous Solids, John Wiley, New York, 1992.
[2] C. Baerlocher, W.M. Meier, D.H. Olson, Atlas of Zeolite Framework Types, fifth ed., Elsevier, Amsterdam, 2002.
[3] J. Kärger, S. Vasenkov, S.M. Auerbach, Diffusion in zeolites, in: S.M. Auerbach, K.A. Carrado, P.K. Dutta (Eds.), Handbook of Zeolite Science and Technology, Marcel Dekker, New York, 2003, pp. 341–422 (Chapter 10).
[4] D. Frenkel, B. Smit, Understanding Molecular Simulations: From Algorithms to Applications, second ed., Academic Press, San Diego, 2002.
[5] A.H. Fuchs, A.K. Cheetham, Adsorption of guest molecules in zeolitic materials: computational aspects, J. Phys. Chem. B 105 (2001) 7375–7383.
[6] B. Smit, R. Krishna, Molecular simulations in zeolitic process design, Chem. Eng. Sci. 58 (2003) 557–568.
[7] R. Krishna, B. Smit, S. Calero, Entropy effects during sorption of alkanes in zeolites, Chem. Soc. Rev. 31 (2002) 185–194.
[8] R.W. Carr, H.W. Dandekar, Adsorption with reaction, in: S. Kulprathipanja (Ed.), Reactive Separation Processes, Taylor & Francis, New York, USA, 2001, pp. 115–154.
[9] H.W. Dandekar, G.A. Funk, R.D. Gillespie, H.A. Zinnen, C.P. McGonegal, M. Kojima, S.H. Hobbs, Process for alkane isomerization using reactive chromatography, UOP Inc., USA, US 5,763,730 (1998).
[10] H.W. Dandekar, G.A. Funk, H.A. Zinnen, Process for separating and recovering multimethyl-branched alkanes, UOP Inc., USA, US 6,069,289 (2000).
[11] L. Song, L.V.C. Rees, Adsorption and transport of *n*-hexane in siliaclite-1 by the frequency response technique, J. Chem. Soc. Faraday Trans. 93 (1997) 649–657.
[12] S. Calero, D. Dubbeldam, R. Krishna, B. Smit, T.J.H. Vlugt, J.F.M. Denayer, J.A. Martens, T.L.M. Maesen, Understanding the role of sodium during adsorption. A force field for alkanes in sodium exchanged faujasites, J. Am. Chem. Soc. 126 (2004) 11377–11386.
[13] D. Dubbeldam, S. Calero, T.J.H. Vlugt, R. Krishna, T.L.M. Maesen, B. Smit, United atom forcefield for alkanes in nanoporous materials, J. Phys. Chem. B 108 (2004) 12301–12313.
[14] R. Krishna, J.M. van Baten, Diffusion of alkane mixtures in zeolites. Validating the Maxwell–Stefan formulation using MD simulations, J. Phys. Chem. B 109 (2005) 6386–6396.
[15] R. Krishna, J.M. van Baten, Influence of isotherm inflection on the diffusivities of C5–C8 linear alkanes in MFI zeolite, Chem. Phys. Lett. 407 (2005) 159–165.
[16] R. Krishna, J.M. van Baten, Linking the loading dependence of the Maxwell–Stefan diffusivity of linear alkanes in zeolites with the thermodynamic correction factor, Chem. Phys. Lett. 420 (2006) 545–549.
[17] R. Krishna, J.M. van Baten, Influence of isotherm inflection on the loading dependence of the diffusivities of *n*-hexane and *n*-heptane in MFI zeolite. Quasi-Elastic Neutron Scattering experiments supplemented by molecular simulations, J. Phys. Chem. B 110 (2006) 2195–2201.
[18] J.M. van Baten, R. Krishna, Entropy effects in adsorption and diffusion of alkane isomers in mordenite: an investigation using CBMC and MD simulations, Microporous Mesoporous Mater. 84 (2005) 179–191.
[19] T.J.H. Vlugt, R. Krishna, B. Smit, Molecular simulations of adsorption isotherms for linear and branched alkanes and their mixtures in silicalite, J. Phys. Chem. B 103 (1999) 1102–1118.
[20] A.L. Myers, J.M. Prausnitz, Thermodynamics of mixed gas adsorption, AIChEJ 11 (1965) 121–130.
[21] C.J. Gump, R.D. Noble, J.L. Falconer, Separation of hexane isomers through nonzeolite pores in ZSM-5 zeolite membranes, Ind. Eng. Chem. Res. 38 (1999) 2775–2781.
[22] R. Krishna, D. Paschek, Permeation of hexane isomers across ZSM-5 zeolite membranes, Ind. Eng. Chem. Res. 39 (2000) 2618–2622.
[23] R. Krishna, R. Baur, Modelling issues in zeolite based separation processes, Sep. Purif. Technol. 33 (2003) 213–254.
[24] D.S. Santilli, Pore probe: a new technique for measuring the concentration of molecules inside porous materials at elevated temperatures, J. Catal. 99 (1986) 335–341.

[25] S. Calero, B. Smit, R. Krishna, Configurational entropy effects during sorption of hexane isomers in silicalite, J. Catal. 202 (2001) 395–401.
[26] R. Krishna, R. Baur, On the Langmuir–Hinshelwood formulation for zeolite catalysed reactions, Chem. Eng. Sci. 60 (2005) 1155–1166.
[27] R. Baur, R. Krishna, A moving bed reactor concept for alkane isomerization, Chem. Eng. J. 109 (2005) 107–113.
[28] O. Talu, Needs, status, techniques and problems with binary gas adsorption experiments, Adv. Colloid Interface Sci. 77 (1998) 227–269.

# Supplementary Data

CBMC simulation results for adsorption of hexane isomers in different zeolites structures at 433 K

# MFI

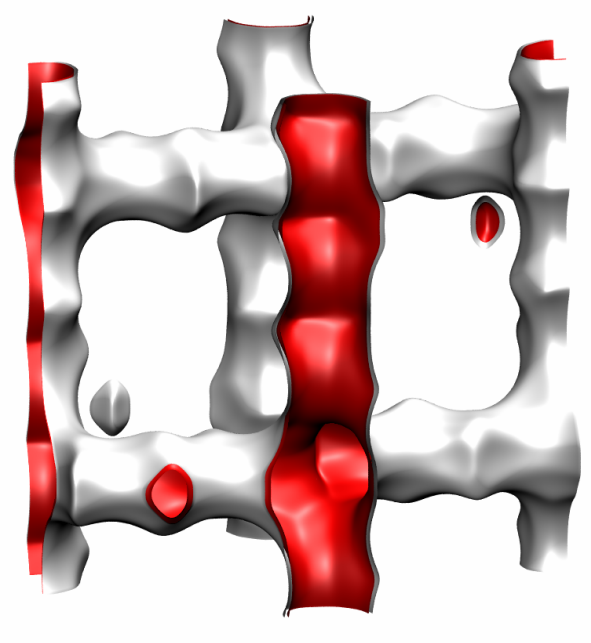

(a)

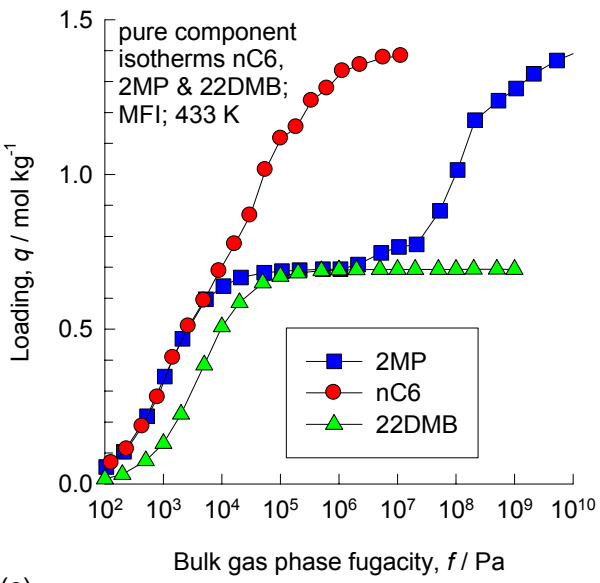
pure component
isotherms nC6,
2MP & 22DMB;
MFI; 433 K
2MP
nC6
22DMB
Loading, q / mol kg-1
Bulk gas phase fugacity, f / Pa

(b)

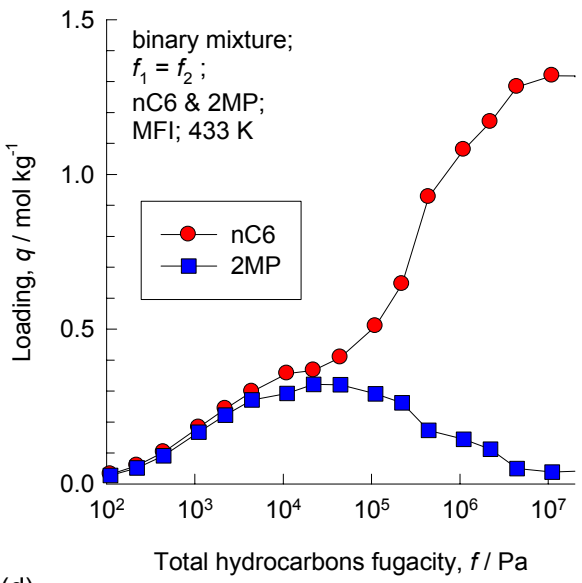
binary mixture;
f1 = f2 ;
nC6 & 2MP;
MFI; 433 K
nC6
2MP
Loading, q / mol kg-1
Total hydrocarbons fugacity, f / Pa

(c)

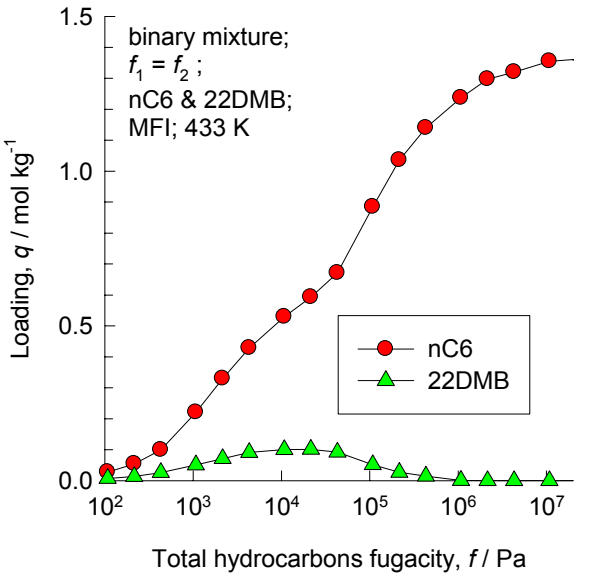
binary mixture;
f1 = f2 ;
nC6 & 22DMB;
MFI; 433 K
nC6
22DMB
Loading, q / mol kg-1
Total hydrocarbons fugacity, f / Pa

(d)

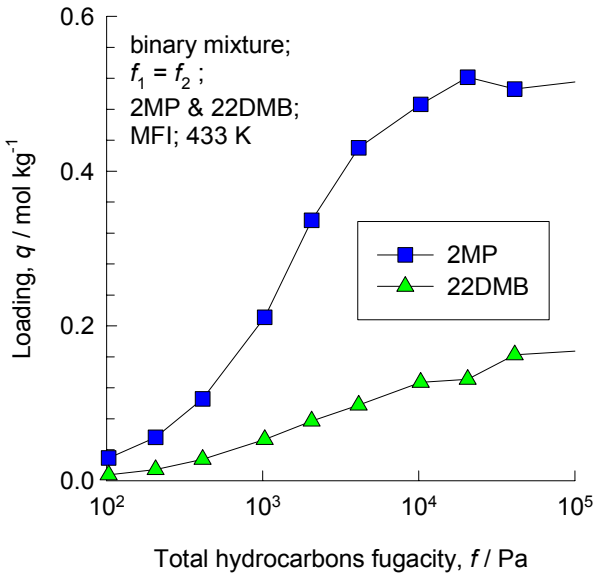
binary mixture;
f1 = f2 ;
2MP & 22DMB;
MFI; 433 K
2MP
22DMB
Loading, q / mol kg-1
Total hydrocarbons fugacity, f / Pa

(e)

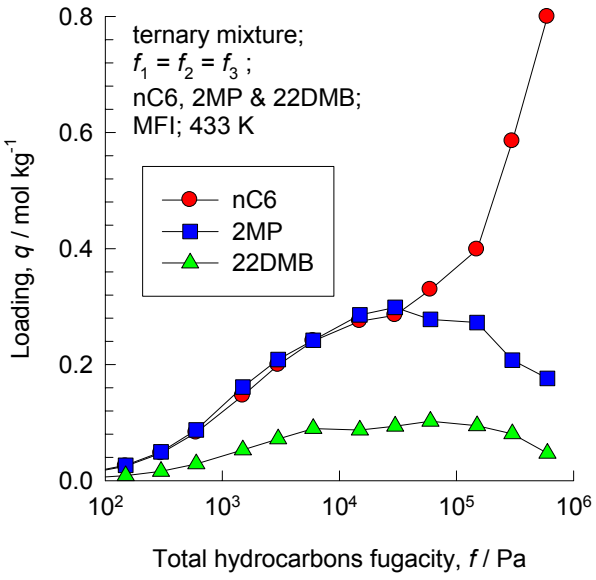
ternary mixture;
f1 = f2 = f3 ;
nC6, 2MP & 22DMB;
MFI; 433 K
nC6
2MP
22DMB
Loading, q / mol kg-1
Total hydrocarbons fugacity, f / Pa

MFI, nC6, 100 kPa, 433 K

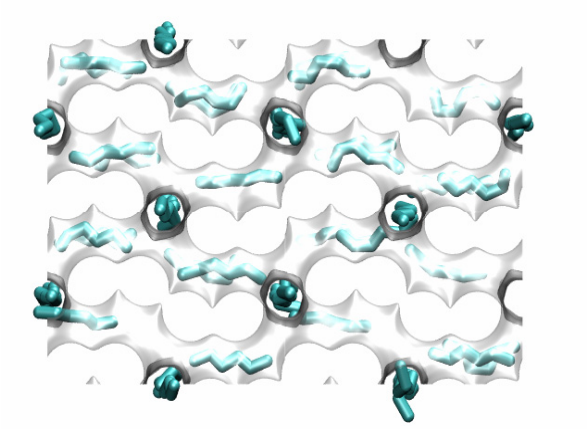

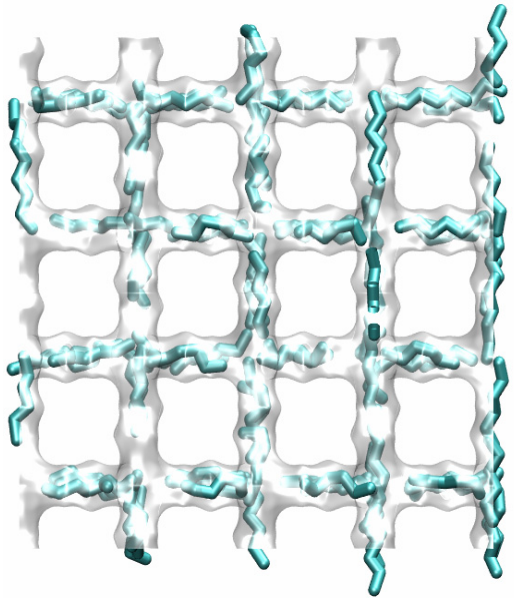

MFI, 2MP, 100 kPa, 433 K

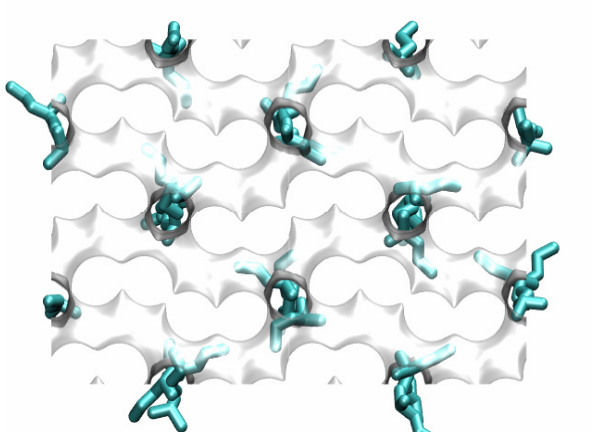

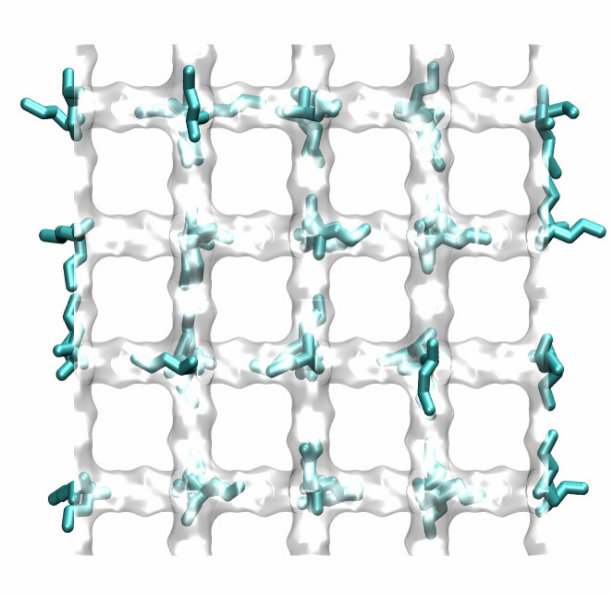

MFI, 22DMB, 10 kPa, 433 K

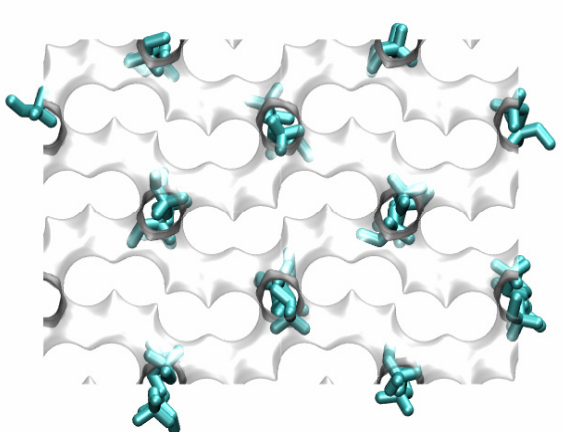

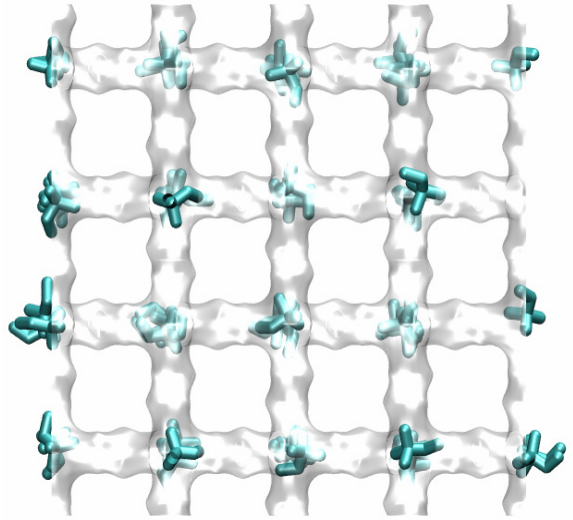

MFI, nC6

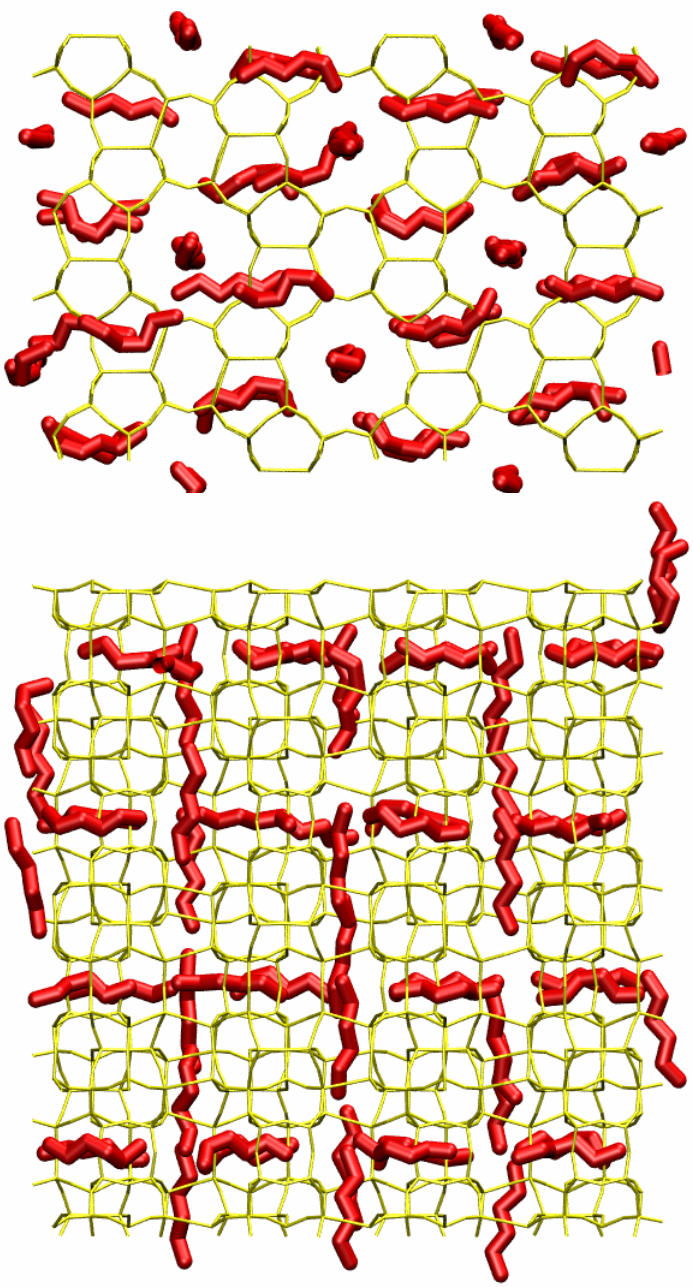

MFI, 22DMB

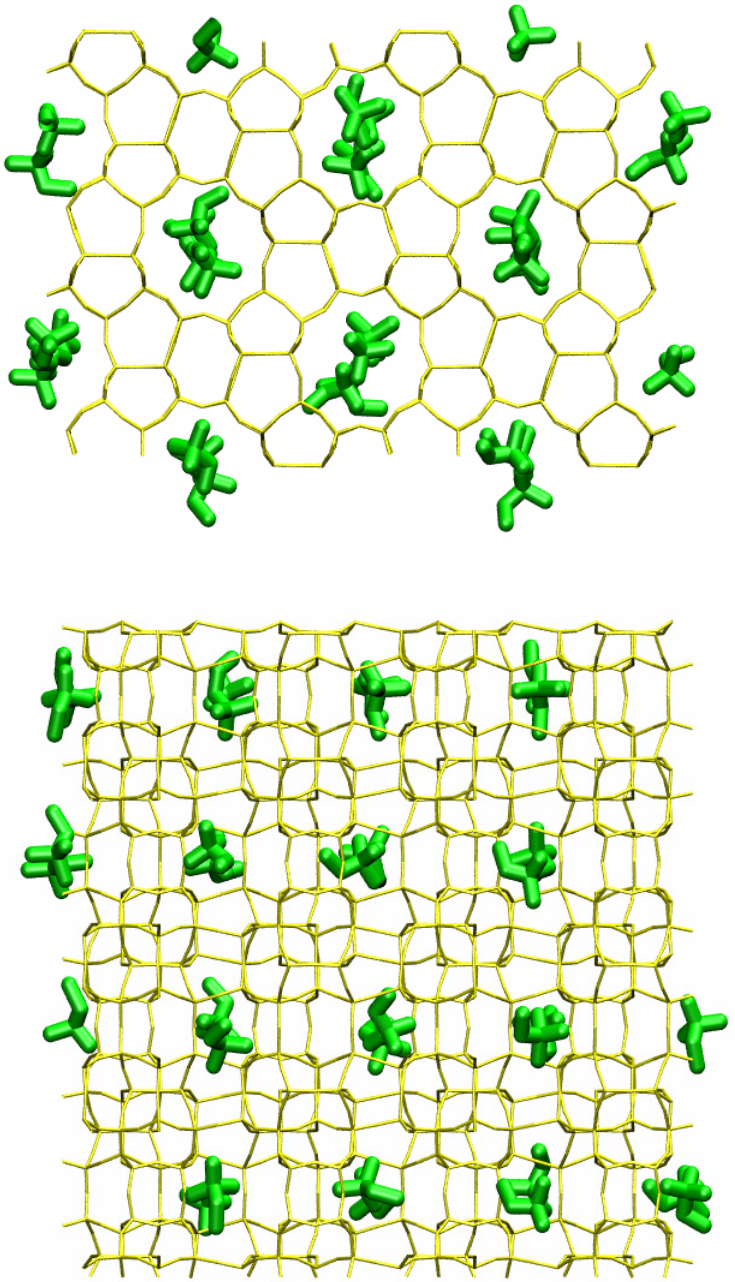

MFI, nC6/22DMB

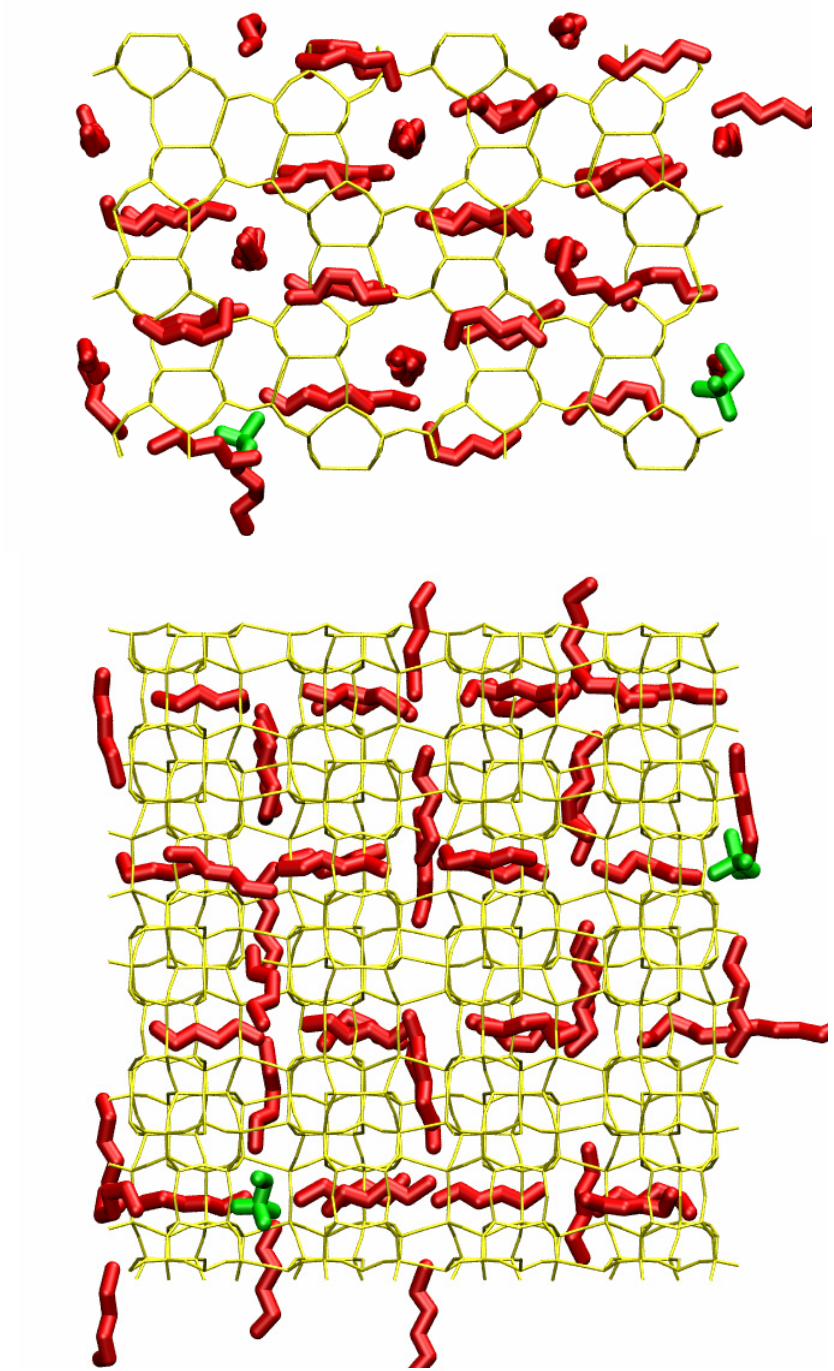

MFI, nC6

MFI, 2MP

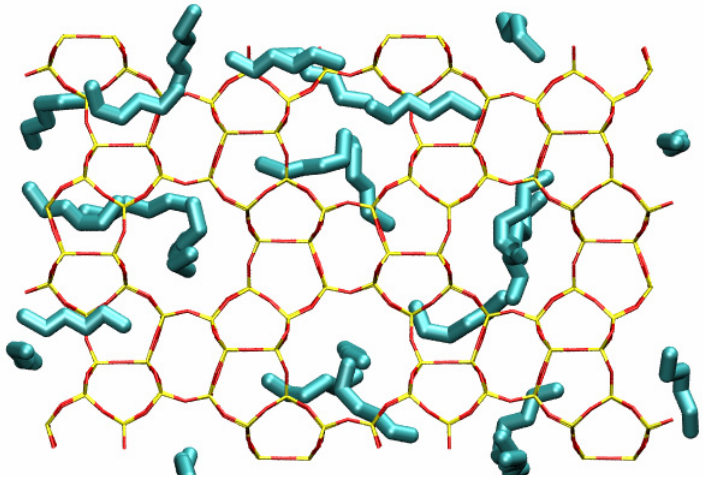

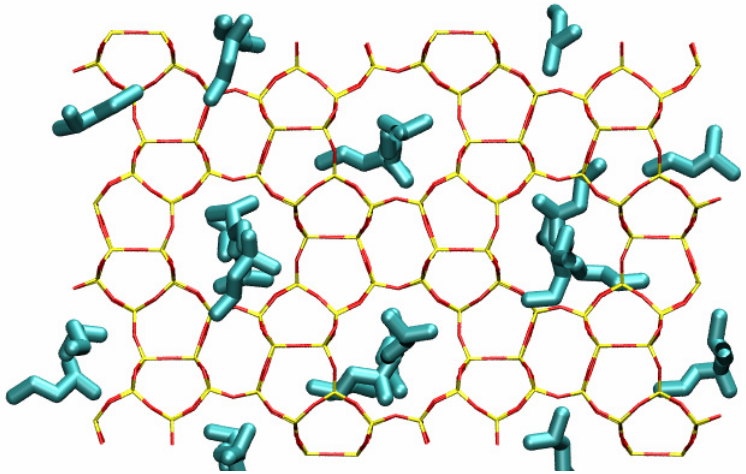

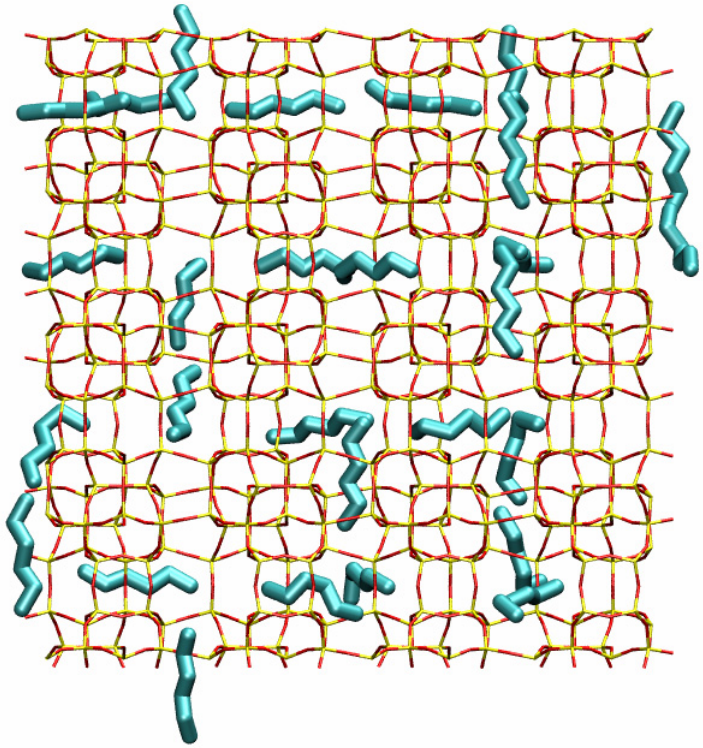

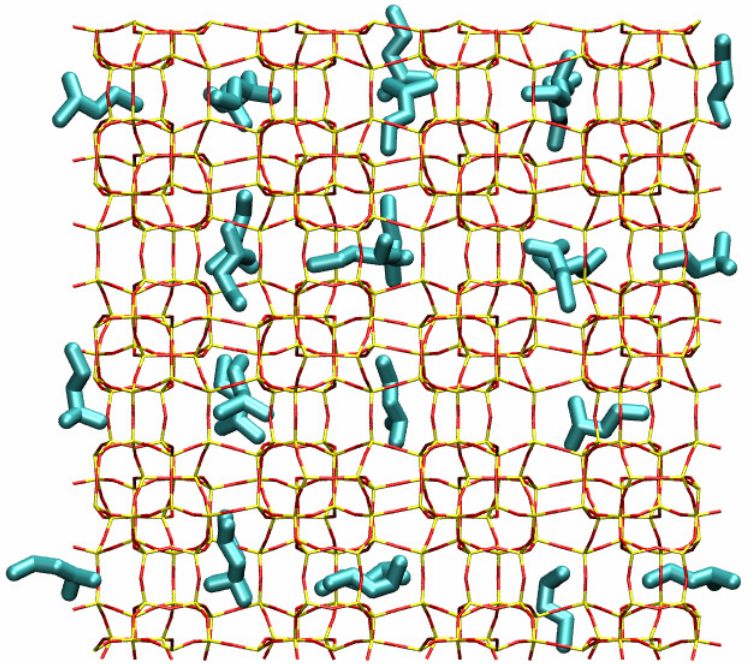

MFI, nC6/2MP

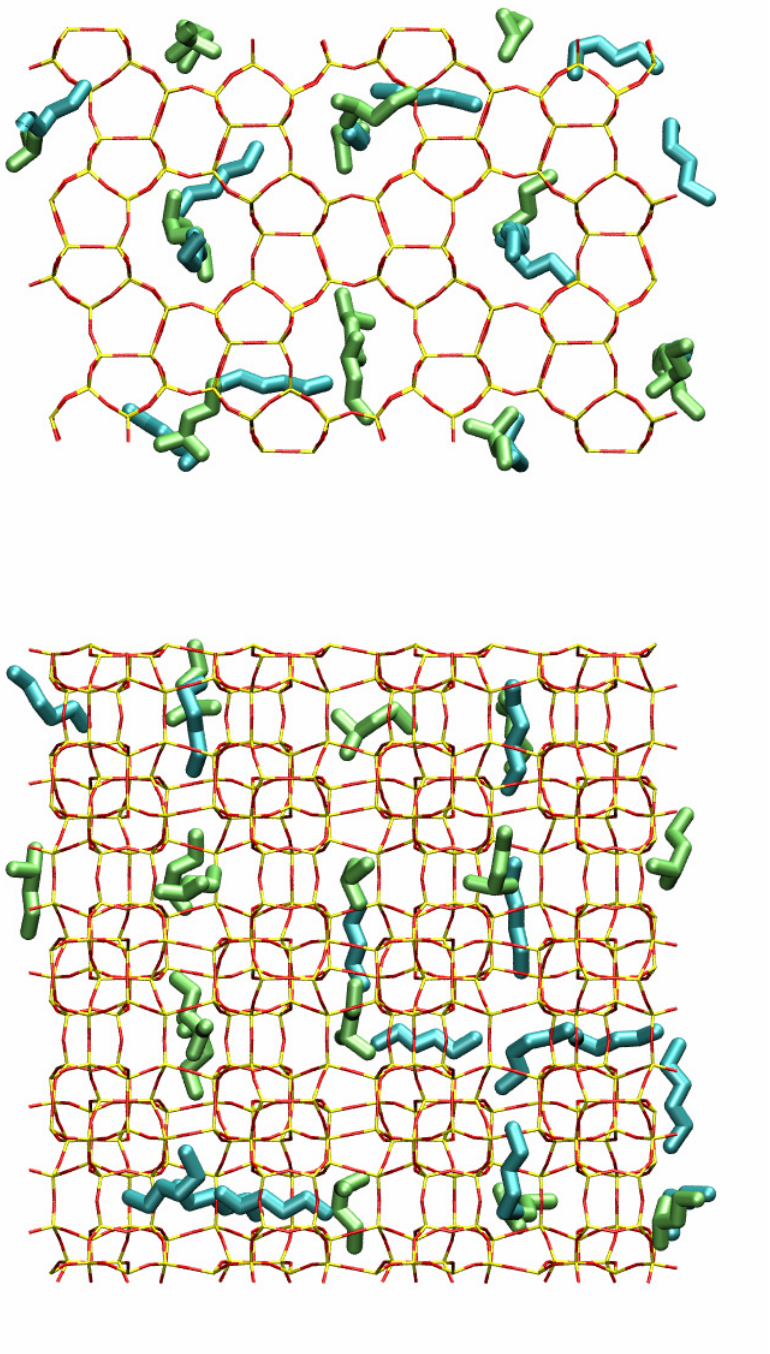

# AFI

(a)

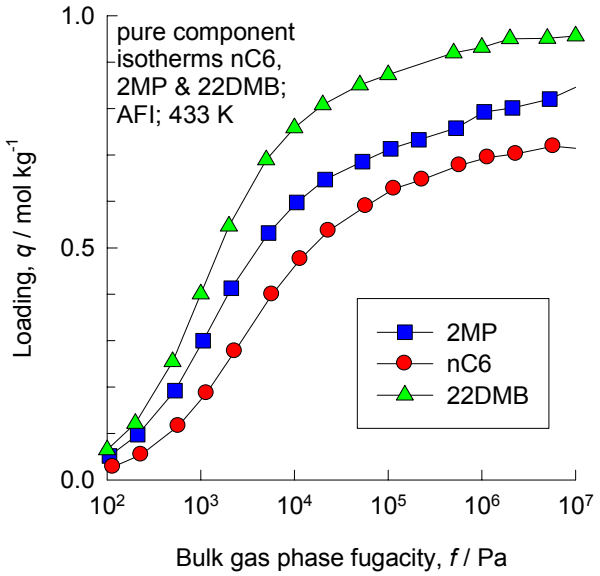
pure component
isotherms nC6,
2MP & 22DMB;
AFI; 433 K
2MP
nC6
22DMB
Loading, q / mol kg-1
Bulk gas phase fugacity, f / Pa

(b)

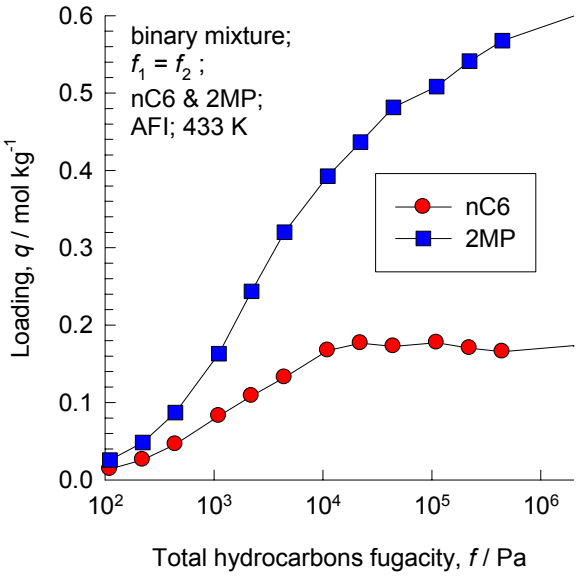
binary mixture;
f1 = f2 ;
nC6 & 2MP;
AFI; 433 K
nC6
2MP
Loading, q / mol kg-1
Total hydrocarbons fugacity, f / Pa

(c)

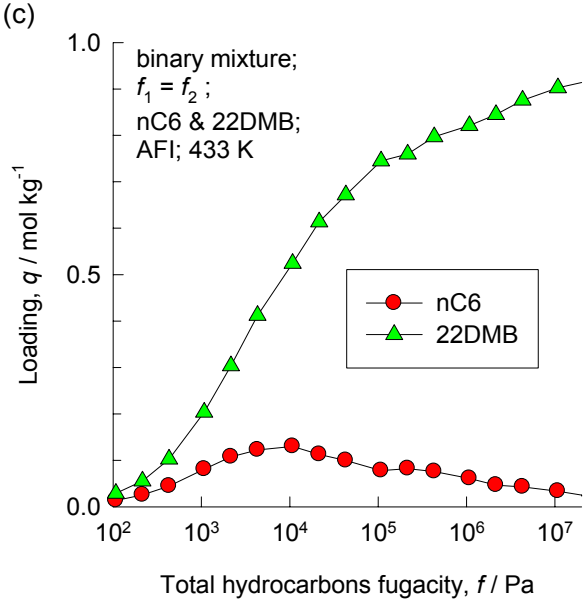
binary mixture;
f1 = f2 ;
nC6 & 22DMB;
AFI; 433 K
nC6
22DMB
Loading, q / mol kg-1
Total hydrocarbons fugacity, f / Pa

(d)

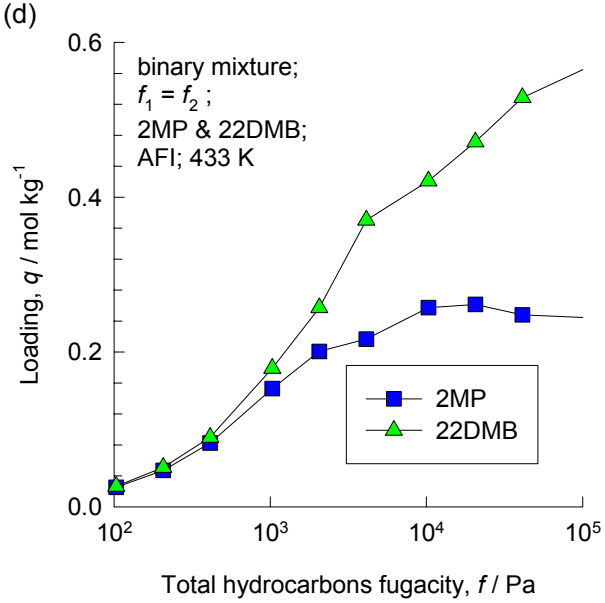
binary mixture;
f1 = f2 ;
2MP & 22DMB;
AFI; 433 K
2MP
22DMB
Loading, q / mol kg-1
Total hydrocarbons fugacity, f / Pa

(e)

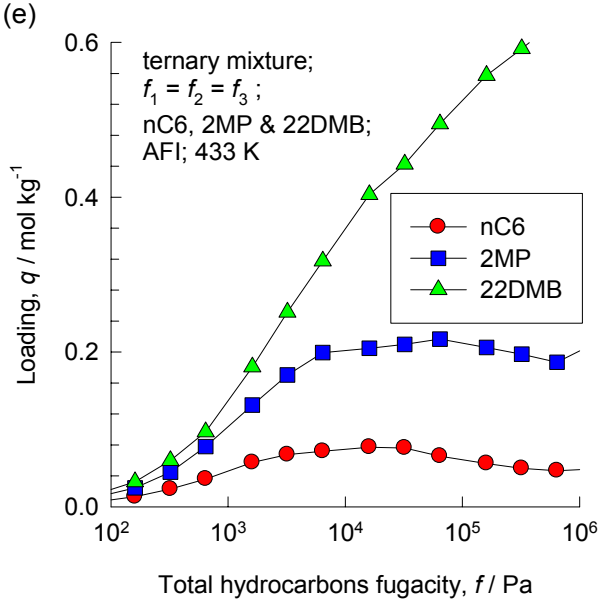
ternary mixture;
f1 = f2 = f3 ;
nC6, 2MP & 22DMB;
AFI; 433 K
nC6
2MP
22DMB
Loading, q / mol kg-1
Total hydrocarbons fugacity, f / Pa

AFI, nC6, 100 kPa

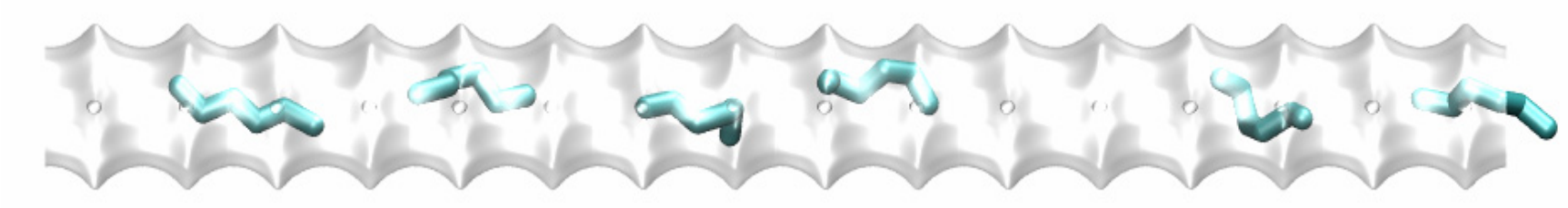

AFI, 2MP, 100 kPa

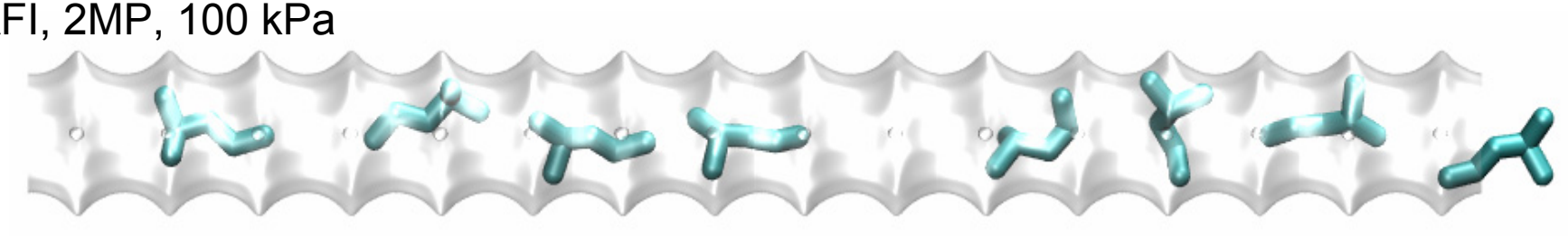

AFI, 22DMB, 10 kPa

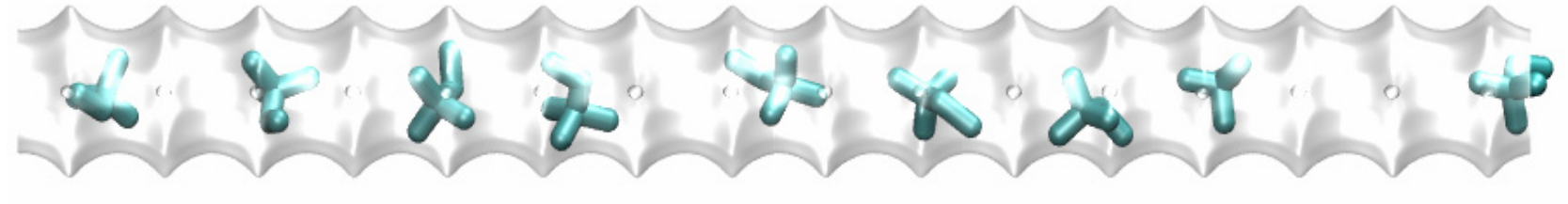

AFI, 22DMB, 100 kPa

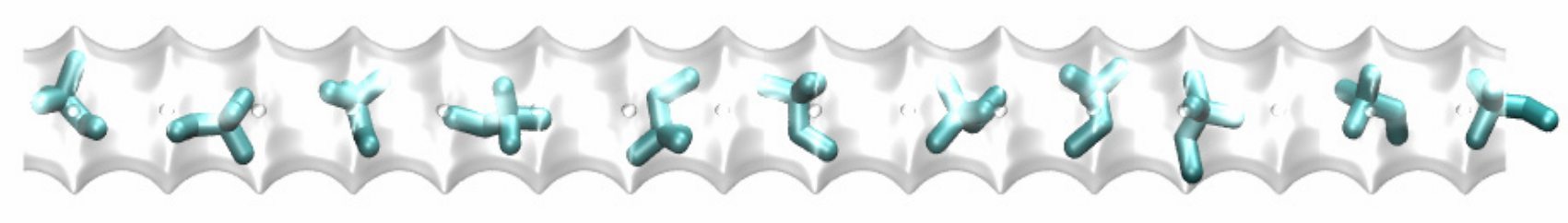

# LTL

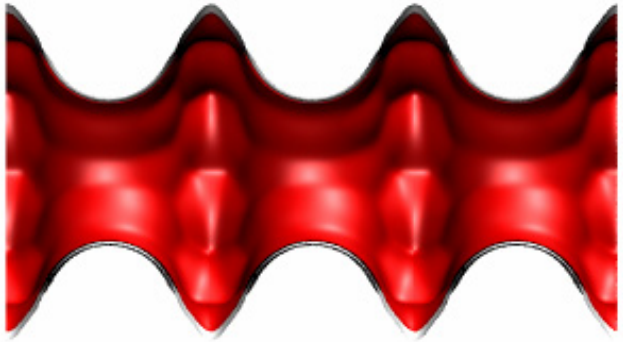

(a)

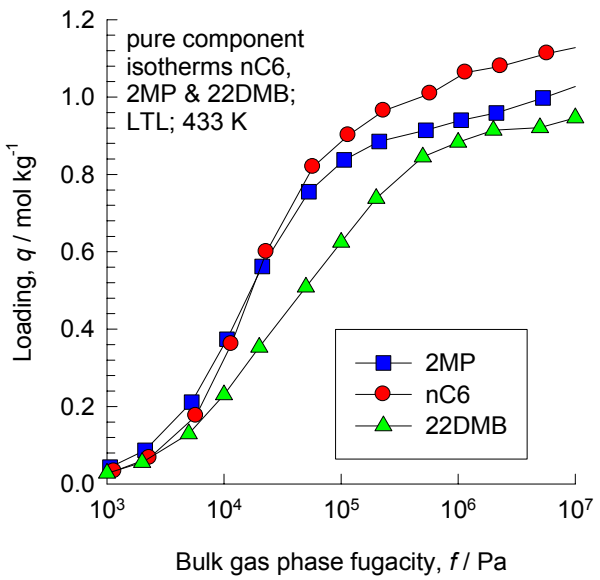
pure component
isotherms nC6,
2MP & 22DMB;
LTL; 433 K
2MP
nC6
22DMB
Loading, q / mol kg-1
Bulk gas phase fugacity, f / Pa

(b)

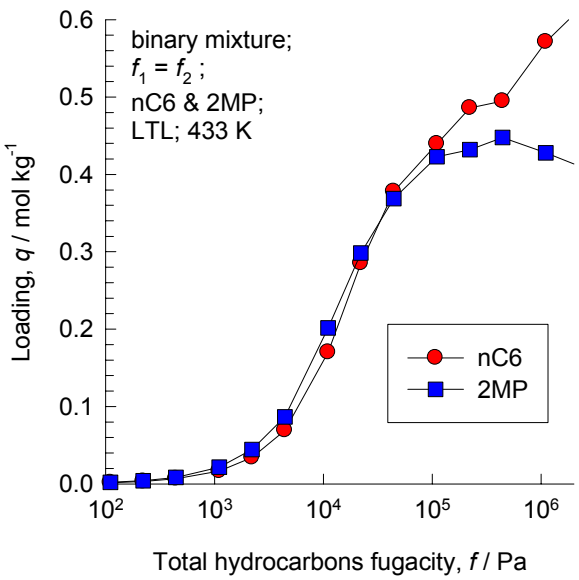
binary mixture;
f1 = f2 ;
nC6 & 2MP;
LTL; 433 K
nC6
2MP
Loading, q / mol kg-1
Total hydrocarbons fugacity, f / Pa

(c)

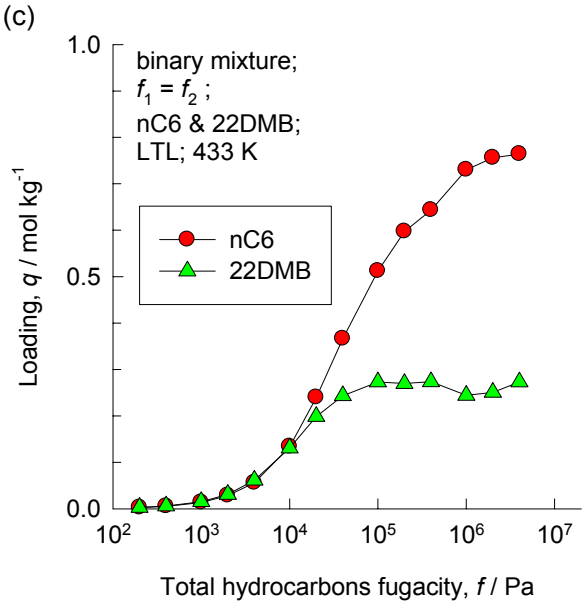
binary mixture;
f1 = f2 ;
nC6 & 22DMB;
LTL; 433 K
nC6
22DMB
Loading, q / mol kg-1
Total hydrocarbons fugacity, f / Pa

(d)

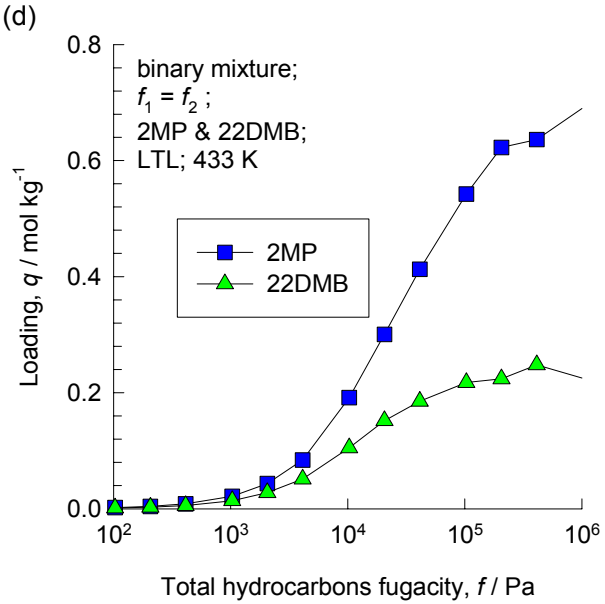
binary mixture;
f1 = f2 ;
2MP & 22DMB;
LTL; 433 K
2MP
22DMB
Loading, q / mol kg-1
Total hydrocarbons fugacity, f / Pa

(e)

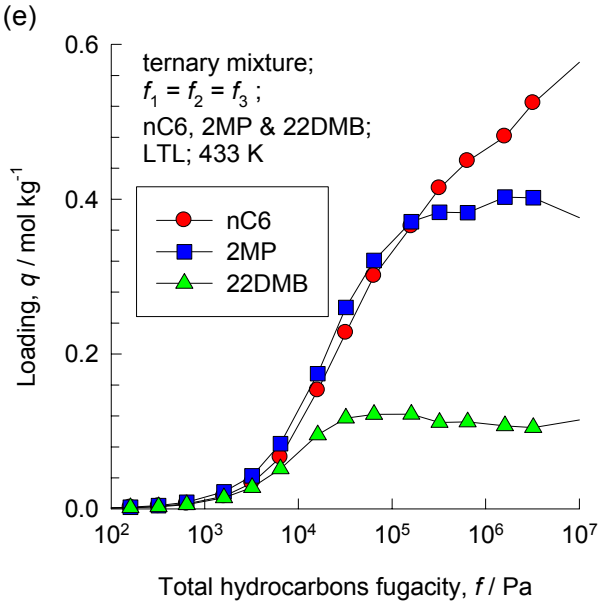
ternary mixture;
f1 = f2 = f3 ;
nC6, 2MP & 22DMB;
LTL; 433 K
nC6
2MP
22DMB
Loading, q / mol kg-1
Total hydrocarbons fugacity, f / Pa

LTL, nC6, 100 kPa

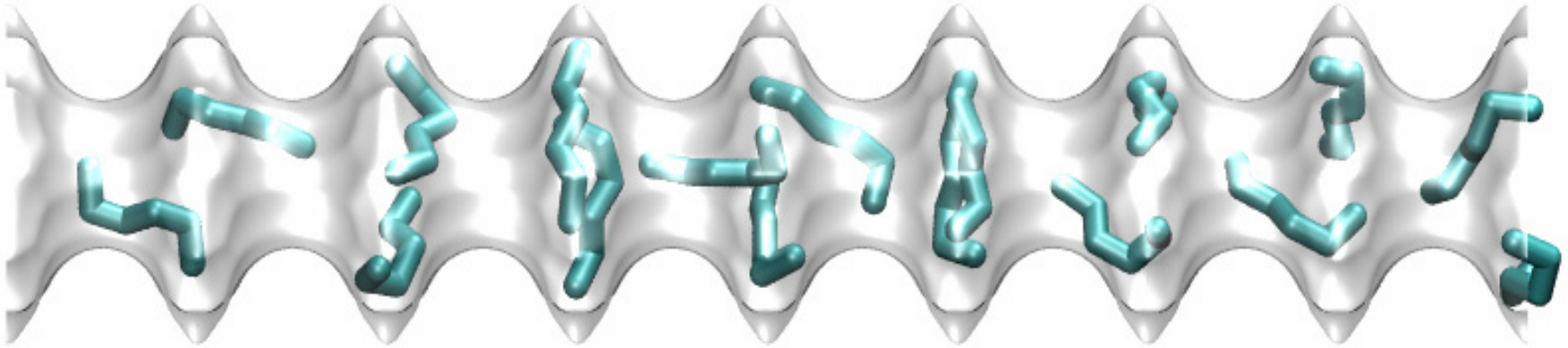

LTL, 2MP, 100 kPa

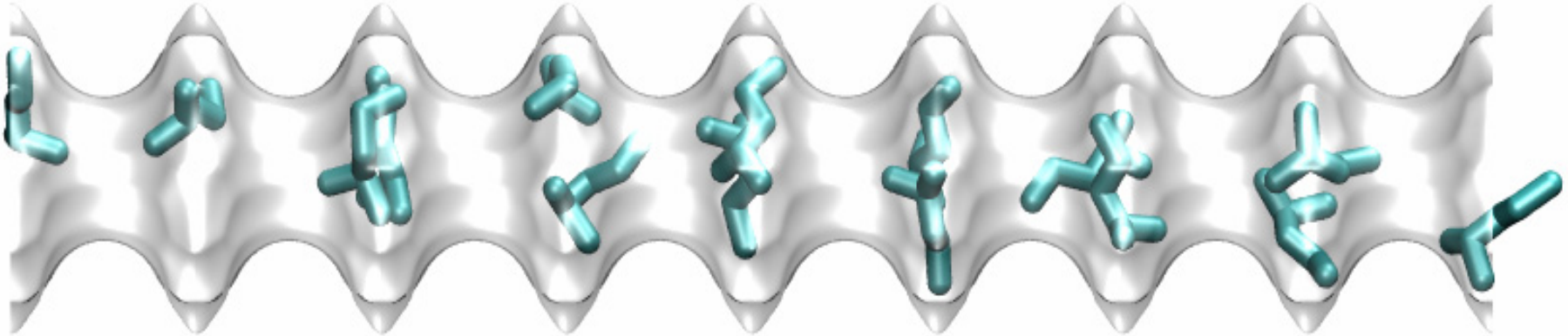

LTL, 22DMB, 100 kPa

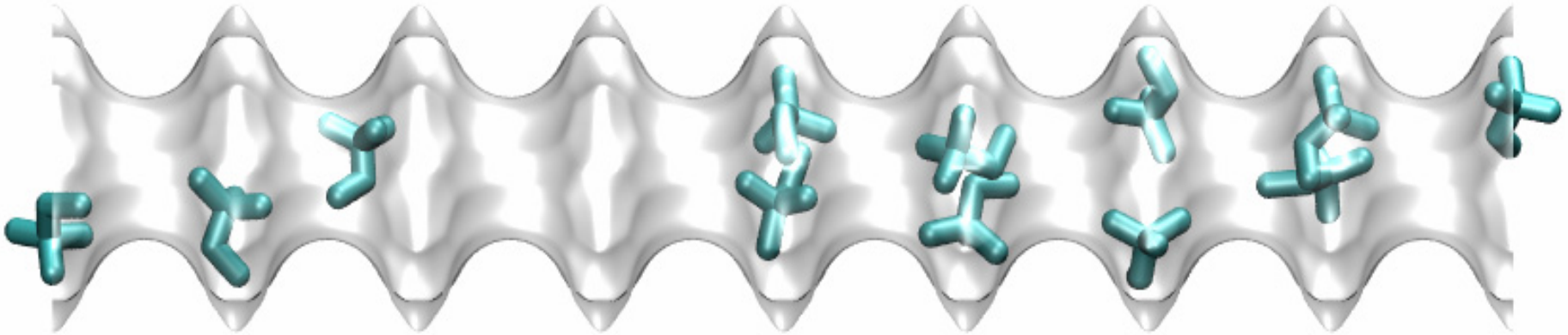

# MOR

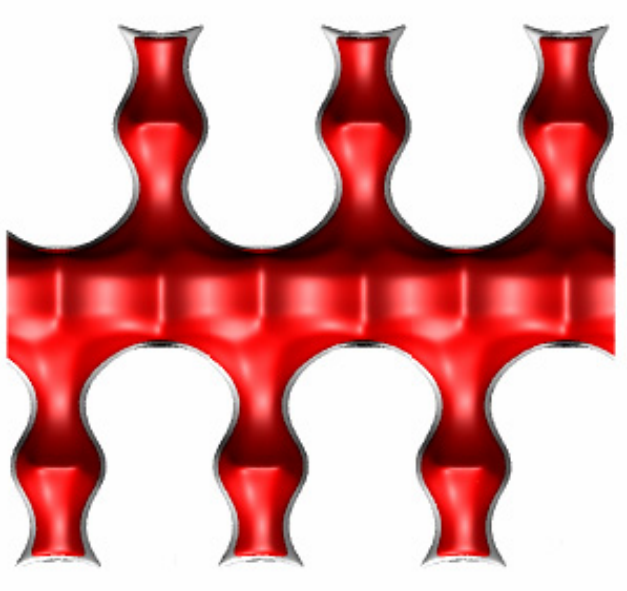

(a)

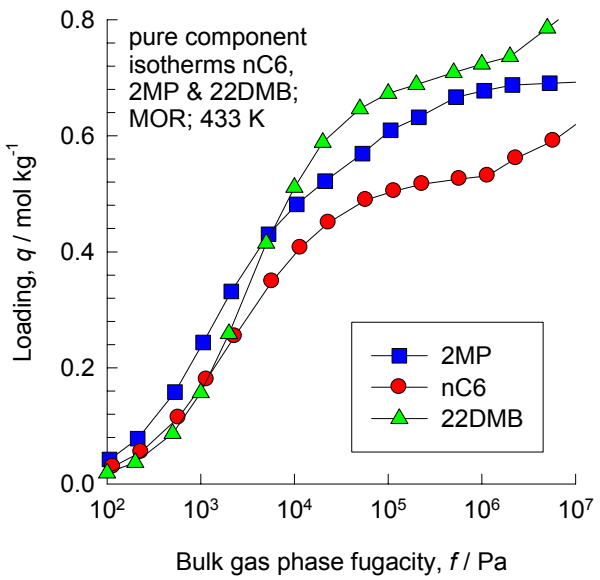
pure component
isotherms nC6,
2MP & 22DMB;
MOR; 433 K
2MP
nC6
22DMB
Loading, q / mol kg-1
Bulk gas phase fugacity, f / Pa

(b)

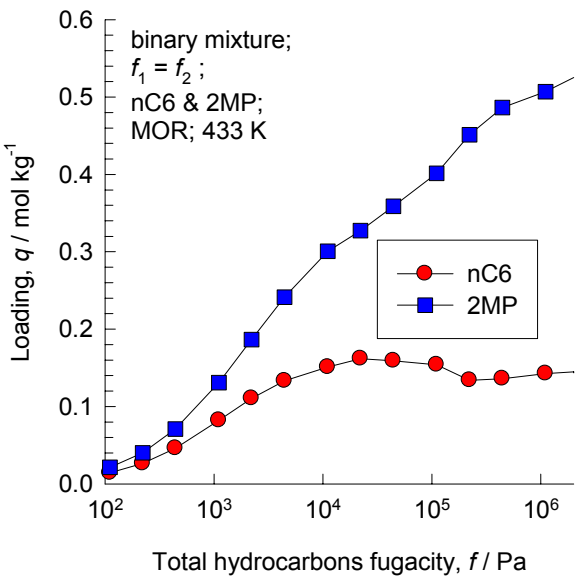
binary mixture;
f1 = f2 ;
nC6 & 2MP;
MOR; 433 K
nC6
2MP
Loading, q / mol kg-1
Total hydrocarbons fugacity, f / Pa

(c)

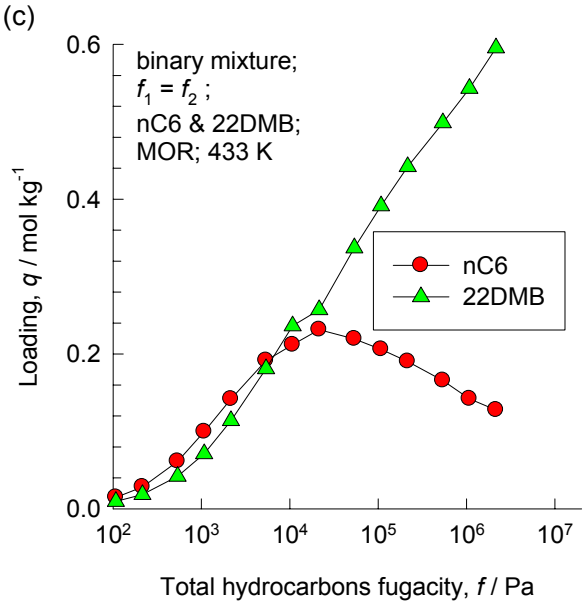
binary mixture;
f1 = f2 ;
nC6 & 22DMB;
MOR; 433 K
nC6
22DMB
Loading, q / mol kg-1
Total hydrocarbons fugacity, f / Pa

(d)

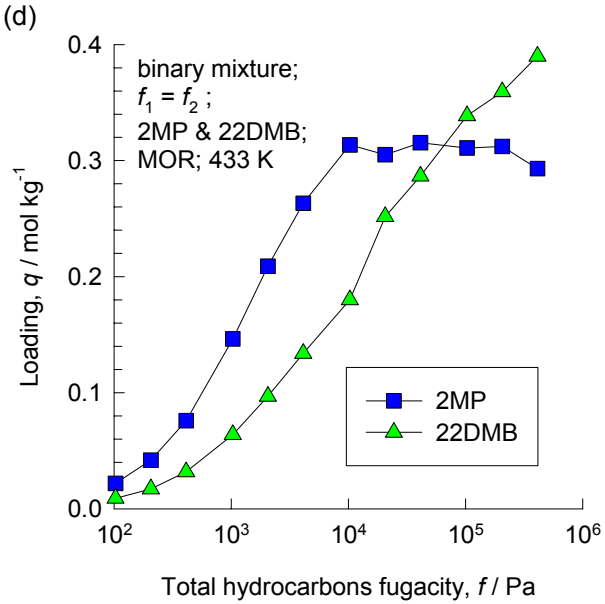
binary mixture;
f1 = f2 ;
2MP & 22DMB;
MOR; 433 K
2MP
22DMB
Loading, q / mol kg-1
Total hydrocarbons fugacity, f / Pa

(e)

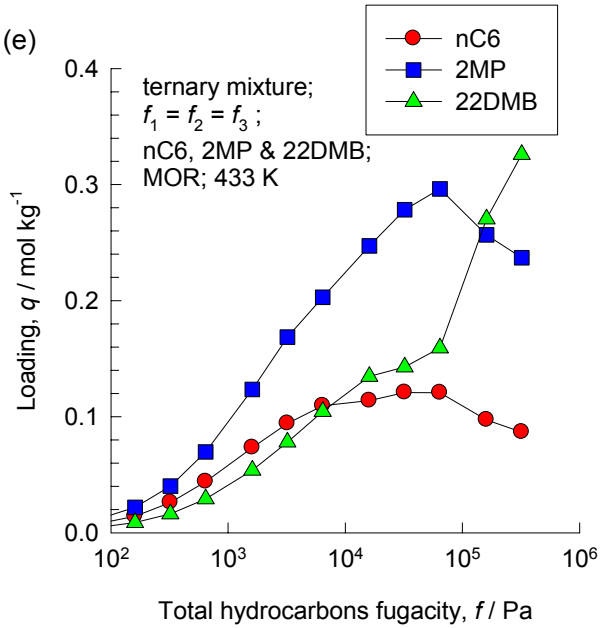
ternary mixture;
f1 = f2 = f3 ;
nC6, 2MP & 22DMB;
MOR; 433 K
nC6
2MP
22DMB
Loading, q / mol kg-1
Total hydrocarbons fugacity, f / Pa

MOR, nC6, 100 kPa

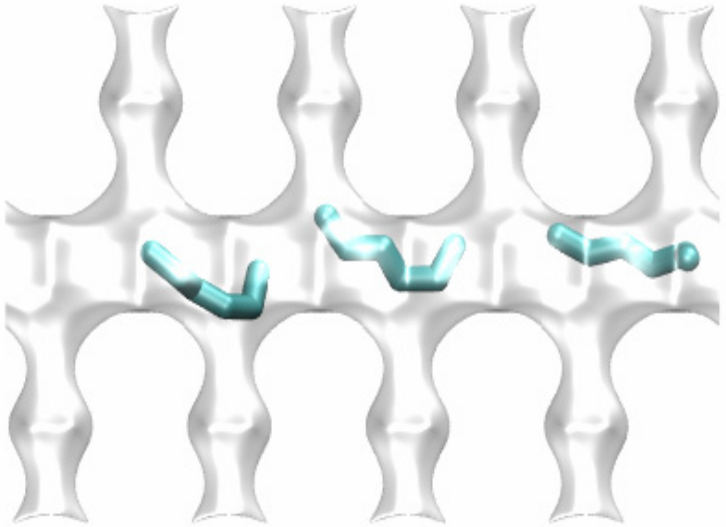

MOR, 2MP, 100 kPa

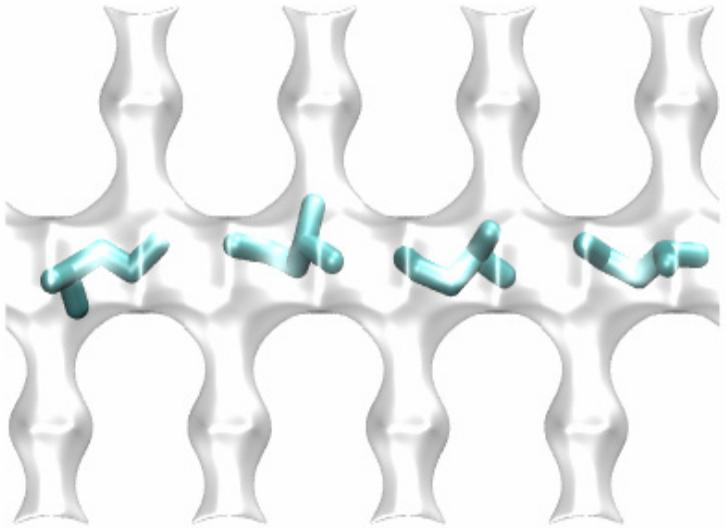

MOR, 22DMB, 100 kPa

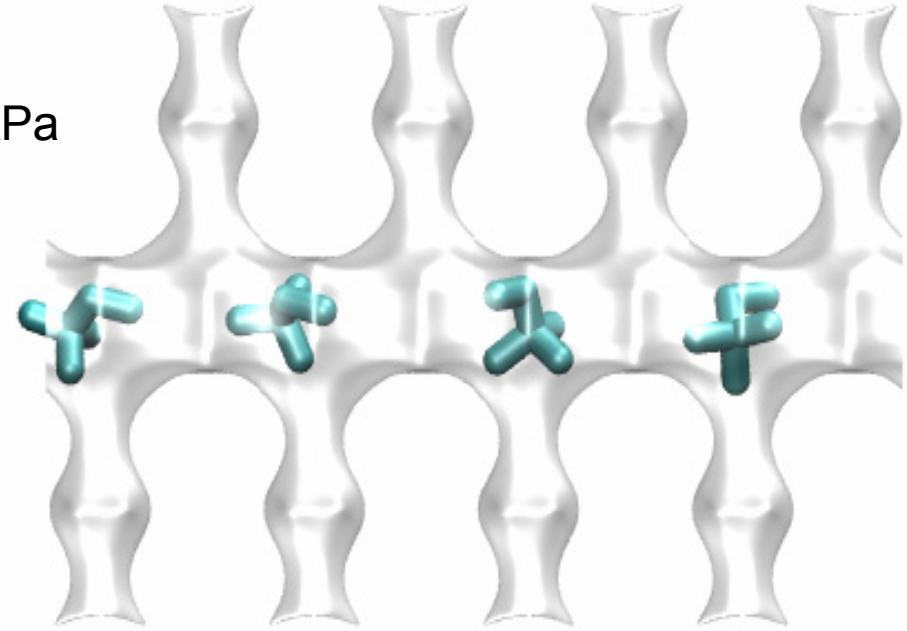

# FAU

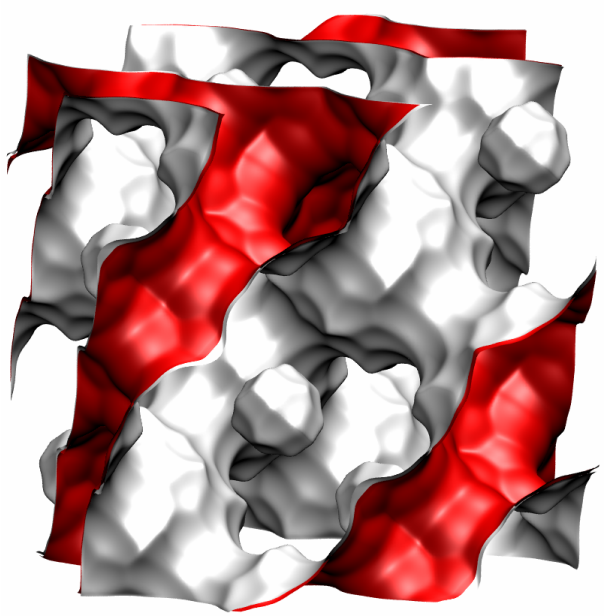

(a)

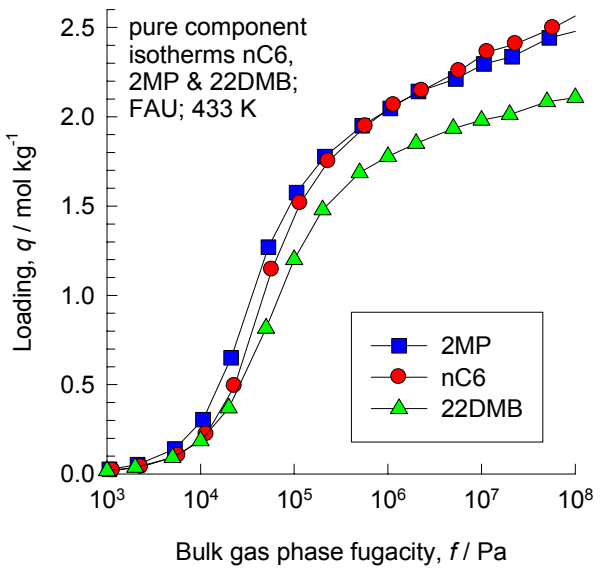
pure component
isotherms nC6,
2MP & 22DMB;
FAU; 433 K
2MP
nC6
22DMB
Loading, q / mol kg-1
Bulk gas phase fugacity, f / Pa

(b)

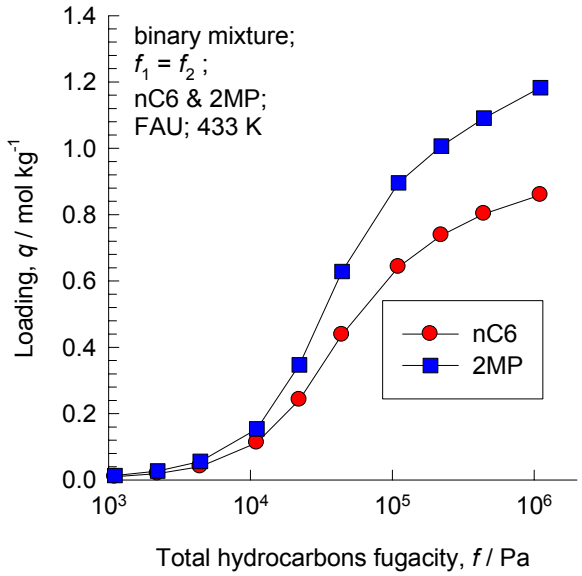
binary mixture;
f1 = f2 ;
nC6 & 2MP;
FAU; 433 K
nC6
2MP
Loading, q / mol kg-1
Total hydrocarbons fugacity, f / Pa

(c)

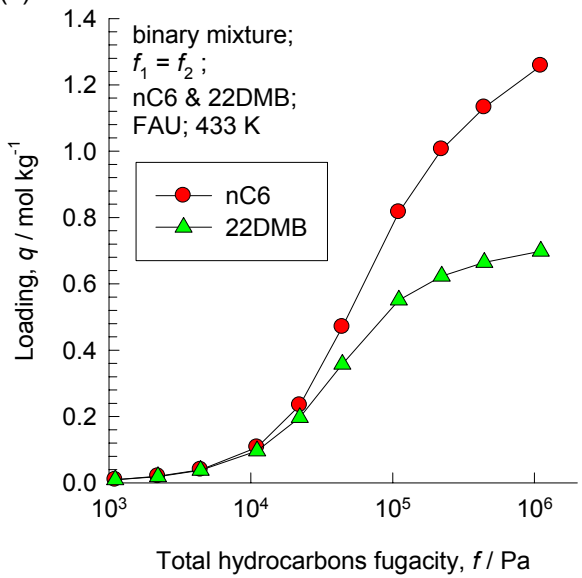
binary mixture;
f1 = f2 ;
nC6 & 22DMB;
FAU; 433 K
nC6
22DMB
Loading, q / mol kg-1
Total hydrocarbons fugacity, f / Pa

(d)

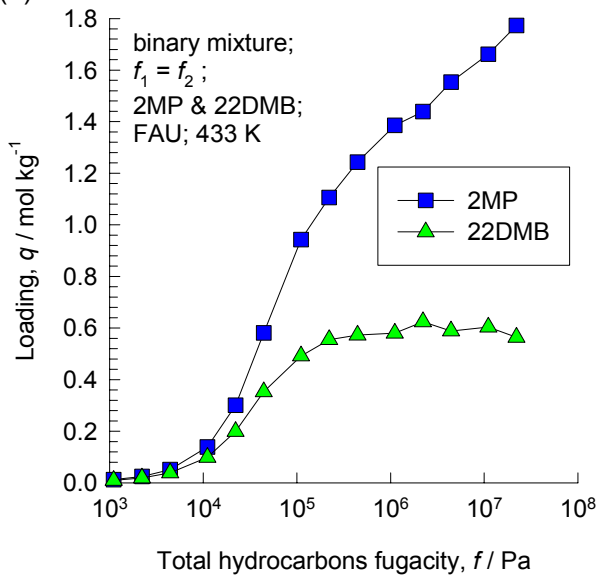
binary mixture;
f1 = f2 ;
2MP & 22DMB;
FAU; 433 K
2MP
22DMB
Loading, q / mol kg-1
Total hydrocarbons fugacity, f / Pa

(e)

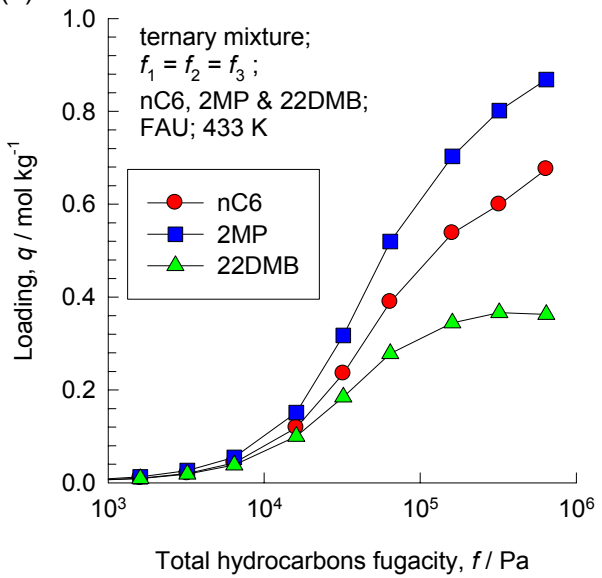
ternary mixture;
f1 = f2 = f3 ;
nC6, 2MP & 22DMB;
FAU; 433 K
nC6
2MP
22DMB
Loading, q / mol kg-1
Total hydrocarbons fugacity, f / Pa

FAU, nC6, 433 K

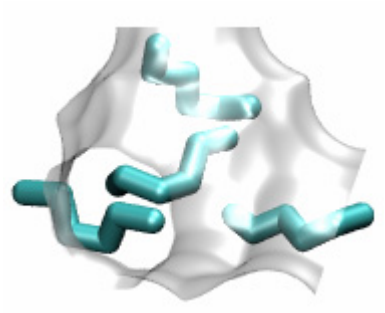

1000 kPa

FAU, 2MP, 433 K

1000 kPa

# Comparison of sorption selectivities at 433 K in various zeolites

based on simulations of the three binary pairs in mixture

based on ternary simulations